Master Thesis

# Modeling and Simulation of Read Distance Enhanced Active Backscattering in UHF RFID Systems

Paul Wiegele

---

Institute of Microwave and Photonic Engineering
Graz University of Technology
Prof. Dr. Wolfgang Bösch




Supervisor: Prof. Dr. Erich Leitgeb
External Supervisor: Dipl.-Ing. Günter Hofer

Graz, October 2013

# Abstract

The Radio Frequency Identification (RFID) technology is said to be one of the fastest emerging markets in the wireless communication sector. From simple object identification in logistics to monitoring of the human vital signs, the number of applications seems endless. This thesis is focused on the RFID technology operating in the Ultra High Frequency (UHF) frequency band.

In the most simple case an RFID communication comprises a reader and a transponder that stores an identification number. Depending on the respective application we can distinguish different tag realizations. Passive RFID tags are solely powered by the surrounding field that is send out via the RFID reader. They are not equipped with any additional power source making them a perfect fit for low-cost one way application. In contrast to semi-passive RFID tags, which are shipped with an additional power source. This allows them to power the internal signal processing blocks independently from the external field. Due to this fact semi-passive tags achieve an excellent receiving sensitivity which is noticeable as an increase in the manufacturing costs. The communication between reader and tag is often limited due to the receiving sensitivity of the RFID reader.

The main aim of this thesis is the analysis of the limiting factor of an RFID communication. This requires the modeling of an RFID communication system that properly reflect the properties of its real life counterpart. A too simple model allows short simulation times but sometimes poorly represents the practical realization. It is important to find a well balanced model. This thesis investigates the possibilities at the tag side to increase the read range.

Once we figured out the limiting factors, we explore three different approaches to enhance the read distance. One approach is focused on the impedance matching between tag antenna and the tag integrated circuit. Using the principle of interference we like to increase the signal power of the backscattered signal. The third approach is focused on an active backscattering architecture that uses a phase locked loop (PLL).

Simulation of the above mentioned systems are carried out to evaluate their technical feasibility. The performance of each approach is evaluated and the pros and cons are discussed.

# Kurzfassung

In letzter Zeit gewinnt im Bereich der drahtlosen Kommunikation die RFID (radio-frequency identification) Technologie immer mehr an Bedeutung. Die Anwendungsmöglichkeiten reichen von Objektidentifikation, zu Anwendungen im Medizinsektor bei der Überwachung lebenswichtiger Körperfunktionen. Diese Arbeit beschäftigt sich mit der RFID Technologie welche im UHF (ultra-high frequency) Bereich arbeitet.

Im einfachsten Fall besteht eine RFID Kommunikation aus einem Lesegerät und einem RFID Transponder der eine Identifikationsnummer besitzt. Je nach Anwendung kommen dabei bestimmte Ausführungen von RFID Transponder zum Einsatz. Passive RFID Transponder versorgen sich ausschließlich durch das elektromagnetisch Feld versorgt, welches vom RFID-Leser ausgesendet wird. Aus diesem Grund finden diese Transponder meist Anwendung bei Wegwerfanwendungen. Semi-passive Transponder hingegen werden mit einer zusätzlichen Energiequelle ausgeliefert. Dadurch ist die Energieversorgung von bestimmten Schaltungsteile unabhängig von der äußeren Feldstärke. Dies schlägt sich in erhöhter Eingangsempfindlichkeit der Transponder nieder. Theoretisch ist es dadurch auch möglich eine größere Distanz zwischen Reader und Transponder zu überbrücken. Meist wird dies jedoch durch die Eingangsempfindlichkeit des Readers begrenzt.

Diese Arbeit beschäftigt sich mit der Analyse der Faktoren die eine RFID Kommunikation beschränken. Dazu ist es nötig ein Modell zu entwickeln welches die Realität hinreichend genau abbildet. Ein einfaches Modell zeichnet sich durch eine kürzere Simulationszeit aus. Dabei muss darauf geachtet werden, dass das Modell nicht zu schwach wird um die Realität zu beschreiben. Es werden Methoden diskutiert die zu einer Reichweitenerhöhung verwendet werden können.

Nachdem die Identifikation der reichweitenbeschränkenden Faktoren erfolgt ist, werden drei unterschiedliche Methoden hinsichtlich ihres praktischen Nutzens untersucht. Einer dieser Ansätze beschäftig sich mit der Anpassung der Impedanz zwischen Transponderantenne und der Halbleiterschaltung der Transponder. Weiters wird untersucht, wie es zu einer Verstärkung eines Signals durch Überlagerung eines zweitens kommen kann. Zuletzt wird ein aktives Backscattering System analysiert welches auf dem Grundprinzip einer Phasenregelschleife (PLL) beruht.

Durch Simulation der oben genannten Systeme wird evaluiert, inwiefern diese zur praktischen Umsetzung geeignet sind. Dabei werden Kennwerte und Vor- und Nachteil der jeweiligen Realisierungen diskutiert.

Deutsche Fassung:
Beschluss der Curricula-Kommission für Bachelor-, Master- und Diplomstudien vom 10.11.2008
Genehmigung des Senates am 1.12.2008

## EIDESSTATTLICHE ERKLÄRUNG

Ich erkläre an Eides statt, dass ich die vorliegende Arbeit selbstständig verfasst, andere als die angegebenen Quellen/Hilfsmittel nicht benutzt, und die den benutzten Quellen wörtlich und inhaltlich entnommene Stellen als solche kenntlich gemacht habe.

Graz, am …….  ……..
(Unterschrift)

Englische Fassung:

## STATUTORY DECLARATION

I declare that I have authored this thesis independently, that I have not used other than the declared sources / resources, and that I have explicitly marked all material which has been quoted either literally or by content from the used sources.

…….  ……..
date  (signature)

## Acknowledgments

First I would like to thank Prof. Erich Leitgeb from the Institute of Microwave and Photonic Engineering, at the Graz University of Technology, for supervising my thesis as well as his outstanding support.

Furthermore I would like to express my gratitude to Dipl.-Ing. Gerald Holweg, head of the Contactless and Radio Frequency Exploration (CRE) department of Infineon Technolgies Austria AG, for making it possible to author my thesis in an industrial surrounding with a practical orientation.

I truly appreciate the supervision of Dipl.-Ing Günther Hofer at Infineon Technologies Austria AG in Graz. His inspiring discussions and useful comments aided the writing of this thesis. Great thanks to all my colleagues from the CRE department of Infineon Technologies Austria AG for the enjoyable and creative working climate.

Finally, I would like to thank my parents Emilie and Ignaz Wiegele for making it possible to pursue a technical study. Further on I would like to give thanks for their encouragement and support during my whole life.

Graz, October 2013 Wiegele Paul

# Contents

# List of Figures

# 1 Introduction

This chapter is focused on giving the reader an introduction to RFID systems. It covers the basic principles and technologies of RFID systems which serve as a basis for the understanding of this thesis. Furthermore we point out the motivation behind this work. Finally the thesis outline gives an overview of the organisational structure of this writing.

## 1.1 RFID Systems

RFID stands for Radio Frequency Identification which is one of the fastest growing markets in wireless communication section. Nowadays RFID has a wide range of application scenarios: object identification, security applications, sensing the vital signs of the human body and many more. The emerging of the smart phone technology is said to be an enabler for further adoption of the RFID technology. The number of possible applications seems endless.
With the use of the RFID technology it is possible to identify objects across a larger distance. In comparison to the bar code technology, RFID technology does not require a clear line of sight in order to ensure proper operation. The bar code reader requires the bar code to be properly rotated. Otherwise the bar code will not be recognized. In contrast to bar codes RFID does not dictate the above mentioned requirements.
In the most simple case a RFID communication consists of an reader and an RFID transponder. The RFID reader uses the electro-magnetic field to query the tags that are nearby. There are mainly two different types of RFID technologies that are used in practice. Whereas the individual technologies differ in their operating frequency and the maximum read distance. High-Frequency RFID tags use the principle of magnetic coupling to query the tags. This mechanism is based on two coils that are coupled through the air interface.
The ultra-high frequency RFID technology operates in a different frequency band compared to HF technology. The UHF RFID technology rests on the principle of radiated electro-magnetic waves analogously to the RADAR (RAdio Detection and Ranging) technology. The reader emits an electro-magnetic wave which is reflected by the transponders that are in the vicinity of the reader. In literature the mechanism of modulating the reflected wave is called backscattering which is an essential part of this thesis.
Depending on the field of application there are different types of RFID tag realizations. Passive RFID tags use the surrounding electro-magnetic field for energy harvesting, making them a perfect fit for low-cost one way applications. Semi-passive tags are equipped with an additional power source that allows them to supply essential signal processing blocks. The additional circuit complexity comes at the cost of increased manufacturing costs, in comparison the passive RFID technology.

## 1.2 Motivation and Project Goals

Semi-passive RFID transponders are known for their remarkable receiving sensitivity. Due to this fact the communication from an RFID reader to a semi-passive tag can be easily established. The transponder replies by reflecting the electro-magnetic wave from the reader (backscattering). Since this mechanism depends on the available power, the communication is often bound by the receiving sensitivity of the RFID reader. Amplifying the signal that is backscattered by the tag enables a communication across a larger distance.

## 1.3 Thesis Outline

Chapter 2 introduces the reader to the essential theoretical background required to understand further elaboration of this thesis. Secondly chapter 3 tries to point out application scenarios that underline the practical relevance of active backscattering. Chapter 4 deals with link budget simulations introduced different simulation scenarios including the modeling of different RFID communication systems. Chapter 5 is dedicated to the impact of impedance matching between tag antenna and tag IC . Followed by chapter 6 which shows a possibility to increase the backscattered power of the backscattered signal. After that chapter 7 outlines a possible realization of an active backscattering system. Chapter 8 recaps and summarizes the outcome of the topics discussed in this thesis. Finally chapter 8.2 states some topics that are looking promising to have potential for further research in this area.

# 2 Fundamentals

This chapter focused on giving the reader a theoretical background to understand the topics that are addressed in this thesis. The first part of this chapter deals with basic principles of the RADAR technology, which serves as the working principle of the RFID technology. Since the vast amount of this work is concerned with the simulation of an RFID communication system we have to establish a properly suited theoretical model. This chapter is concluded with the principle of a PLL.

## 2.1 RADAR

World War II can be seen as the main reason for pushing on the development of the RADAR technology. At that time it was mainly used to find out the altitude, location, speed and trajectory of a flying object. Nowadays there exist a vast amount of application utilizing this operating principle.
A typical wireless communication consists of a sender that is emitting an electro-magnetic wave. As the traveling wave approaches an obstacle it is partly reflected towards the sender. By measuring the time it takes for the signal to end up back at the sender, we can determine the distance between them [1]. The figure in 2.1 depicts the above described scenario.

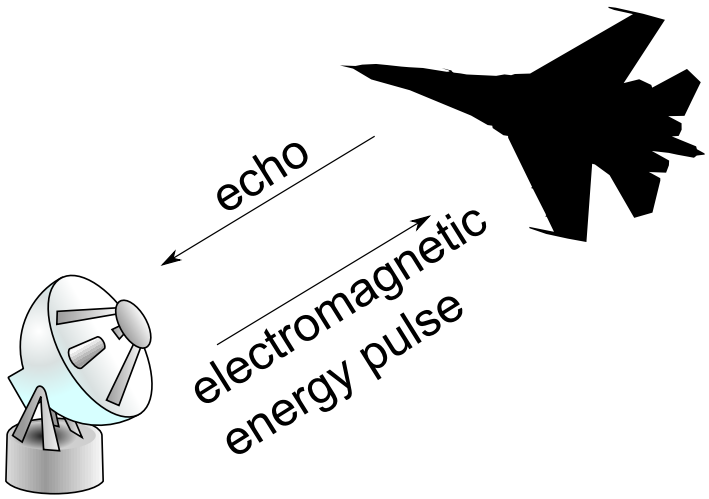


Figure 2.1: Simplified radar principle

[1] assuming the propagation speed of the electro-magnetic impulse is known and stays constant over time

## 2.2 Wireless backscatter radio

Thinking back to the example from section 2.1 we have seen that the radar technology gives us various information on a flying object. Assuming that this technology is used by the military, we currently lack the ability to differentiate between friend or foe. During World War II the German Luftwaffe was using an ingenious trick to get hold of this dilemma. At the time of a battle when the Luftwaffe was fighting against the British, the Luftwaffe simultaneously performed a full rotation[2] with their airplane. As time went by, the British realized that this maneuver is correlated with airborne radar. The cockpits of the Luftwaffe pilots were equipped with a device reporting that they are illuminated by a radar wave. Which was the event that triggered the before mentioned maneuver. To put in another way, they were modifying the RCS telling the ground crew that they are one of them (example taken from [4]). This schema can be seen as one of the earliest forms of a modulated backscatter radio.
The RFID technology relies on the analogous principle as described above. In this case the sender is an RFID reader that emits an electro-magnetic field. The receiver, also called tag or transponder, is placed into the reader's field to establish a communication (see figure 2.2).

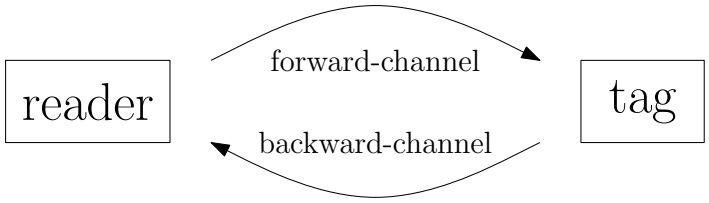


Figure 2.2: Basic UHF RFID communication scenario

The backward-channel (from tag to reader) is based on the principle of a backscatter radio. In the example from section 2.1 we have seen that the portion of the reflected wave depends on the size of the obstacle (area). By varying the effective area (RCS) that is exposed to the reader, the tag is able to use this schema as a backward-channel. This means that the tag modulates the magnitude of the wave that is backscattered to the reader (see figure 2.3). With the use of this principle the tag is able to talk back to the reader.

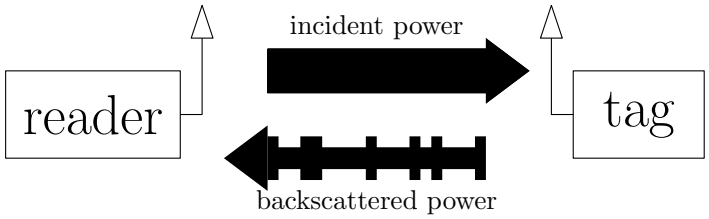


Figure 2.3: RFID UHF backscattering principle

The block diagram in figure 2.2 can be seen as a basis for all further investigations, which is refined during the course of this thesis.

[2] a roll around their longitudinal axis

## 2.3 Inner architecture of an UHF RFID tag

During the course of this thesis we will be concerned about the internal workings of an RFID tag. In order to facilitate the understanding of this work, it is essential to understand the basic building blocks that make up an RFID tag. The figure in 2.4 illustrates the internal structure of an RFID tag. In the left side of the picture there is the tag antenna realized as a dipole. On the right is a gray block that represents the tag IC. The tag IC can be further decomposed into three subcomponents. Starting from left to the right there is the analog block, followed by the state machine and finally the memory. The analog front-end processes the signal from the air interface that is delivered from the tag antenna. Passive tags are solely powered by the energy that is harvested from the surrounding electro-magnetic. This is accomplished with a rectifier circuit that is found within the analog front-end. Other tasks include clock recovery and modulation/demodulation of the data signal. The output of the analog front-end is a digital signal which serves as the input to the state machine. The state machine is a purely digital block, that processes the input signal according to the RFID standard. As the name RFID implies, the main field of application is identification. This implies that each tag is equipped with an individual ID[3]. The memory block is implemented with non-volatile memory, being able to store information even if power supply is lost [6].

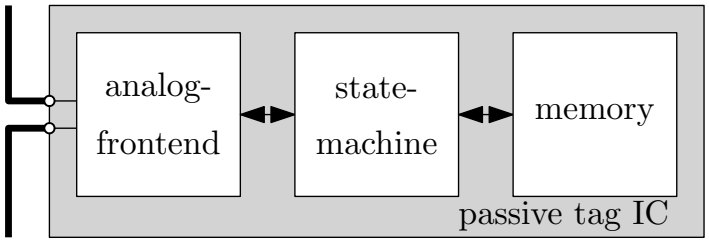


Figure 2.4: Passive RFID UHF tag

The scenario above discussed the internal structure of a passive RFID tag. In case of a semi-passive tag we have an additional power source in form of a battery. With the use of the battery we can assure the power supply of the tag's internal blocks. This means that we do not depend solely on the power that is harvested from the surrounding electro-magnetic field. Figure 2.5 depicts the block diagram of a semi-passive RFID tag. With the use of active envelope demodulation within the analog front-end, we are able to increase the tag's sensitivity. Due to that fact we can increase the distance spanned by the forward-channel. This comes at the cost of increased tag complexity which has to be equipped with a battery [6].

## 2.4 Modeling the communication channel

The radio communication passing the transmission channel is usually distorted. The effects of distortion includes multipath propagation, attenuation, fading, reflection, diffraction and

[3] assuming that the each ID is used only once

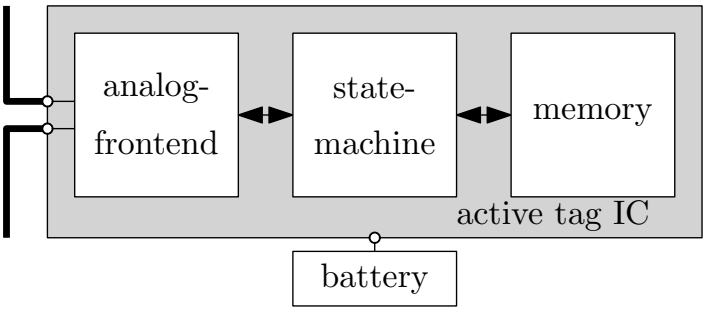


Figure 2.5: Semi-passive RFID UHF tag

noise to name a few. In the most simple case the communication channel is just damping the signal power. For reasons of simplicity we ignore the effects mentioned earlier.

### 2.4.1 FSPL - Free space path loss

This model assumes that the signal sent from the reader to the tag just experiences attenuation. A major simplification made by supposing that the reader behaves like an isotropic radiator (point source). As the name already implies we presume that the propagation medium is vacuum (free space). Since the electro-magnetic radiation is spread out evenly in all directions, we can calculate the intensity S at a certain distance using the formula in 2.1.

$$S = \frac{P_{reader}}{4 \cdot \pi \cdot r^2} \tag{2.1}$$

Where $P_{reader}$ is the transmission power of the reader and $r$ is the distance between reader and tag. Dividing the reader power by the area of a sphere we end up with the intensity at a certain distance $r$. In order to obtain the power that is delivered to the tag, we have to define the area that is exposed towards the reader. Figure 2.6 illustrates the field generated by a point source. As we move away from the center we realize that the area that is spanned by the sphere increases by the power of two. It follows from the forgoing that the intensity drops quadratically as the distance is increased [4].
The power received at the tag depends on the product of the intensity and the effective antenna area.

$$P_{tag} = S \cdot A_{eff} \tag{2.2}$$

The ratio between the power received the transmission power of the reader yields the free space path loss FSPL. Using equation 2.2 and 2.1 we get:

$$FSPL = \frac{P_{reader}}{P_{tag}} = \frac{4 \cdot \pi \cdot r^2}{A_{eff}} \tag{2.3}$$

The literature in [2] and [14] suggests that the effective area $A_{eff}$ of a tag can be approximated with:

$$A_{eff} = \frac{\lambda^2}{4 \cdot \pi} = \frac{c^2}{f^2 \cdot 4 \cdot \pi} \tag{2.4}$$

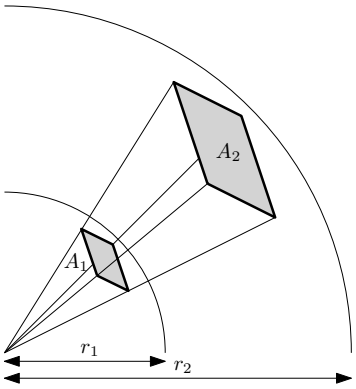


Figure 2.6: Cross section of a field generated by an isotropic radiator

Where $c$ is the speed of light and $f$ is the operating frequency. With the help of equation 2.4 we can rewrite equation 2.3:

$$FSPL = \left(\frac{4 \cdot \pi \cdot r}{\lambda}\right)^2 \tag{2.5}$$

This is just a very rough estimation for calculating the losses introduced by the wireless channel.

### 2.4.2 Friis transmission equation

The Friis transmission equation is named after the Danish-American radio engineer Harald T. Friis from Bell Labs. In its simplest form it looks like this:

$$P_{receiver} = P_{sender} \cdot G_{receiver} \cdot G_{sender} \cdot \left(\frac{\lambda}{4 \cdot \pi \cdot r}\right)^2 \tag{2.6}$$

Where $G_{receiver}$ and $G_{sender}$ are the antenna gain of the respective antennas. To simplify matters we assume that both antennas are isotropic. The rightmost part of equation 2.6 is the inverse of the FSPL which was already derived in the section before. Putting it all together we obtain:

$$P_{receiver} = P_{sender} \cdot \left(\frac{\lambda}{4 \cdot \pi \cdot r}\right)^2 \tag{2.7}$$

We implicitly assume that the sender and the receiver are at least $\frac{\lambda}{2 \cdot \pi}$ apart (far field). Due to that we can safely assume that the field can be characterized in radiative manner. Where $\lambda$ is the wavelength defined as $\frac{c}{f}$. Refining the basic form the Friis equation requires us to look into the details of antenna theory.

### 2.4.3 Generic path loss

Path loss is a more generalized form of the equation used for the free space loss, where the loss exponent n depends on the surrounding medium. The book in [24] gives an overview of

the possible loss exponents for different propagation media. The Friis equation that is based on the free space loss which has a fixed loss exponent of 2, since we assume that the antenna is surrounded by vacuum. Usual values for typical application scenarios are situated between 2-4. For very lossy environments a loss exponent between 4-6 is assumed. Since indoor application scenarios suffer from multipath propagation and absorption the loss exponent is much higher compared to free space loss. Equation 2.8 shows the generic form of the path loss PL equation:

$$PL = \frac{P_{sender}}{P_{receiver}} = \left(\frac{4 \cdot \pi \cdot r}{\lambda}\right)^n \tag{2.8}$$

### 2.4.4 Log-distance path loss model

Due to the dynamic range of the power levels it's often convenient to work with a logarithmic scale. Note what we are using $PL^dB$ to express the path loss in logarithmic domain. Converting both sides of equation 2.8 to logarithmic domain we end up with following equation:

$$\begin{aligned} 10 \cdot log10\left(\frac{P_{sender}}{P_{receiver}}\right) &= 10 \cdot log10\left(\frac{4 \cdot \pi \cdot r}{\lambda}\right)^n \\ P^{dB}_{sender} - P^{dB}_{receiver} &= 10 \cdot n \cdot log10(r) + 10 \cdot n \cdot log10\left(\frac{4 \cdot \pi}{\lambda}\right) \end{aligned}$$

In literature the equation above is referred to as the log-distance path loss model. The path loss exponent is usually determined empirically. Knowing the path loss exponent we can derive a new interpretation of the path loss formula.

$$PL^{dB} = \underbrace{10 \cdot n \cdot log10(r)}_{f(r,n)} + \underbrace{10 \cdot n \cdot log10\left(\frac{4 \cdot \pi}{\lambda}\right)}_{const.\ d(n)} \tag{2.9a}$$

$$= k \cdot log10(r) + d(n) = \frac{\Delta y}{\Delta x} \cdot log10(r) + d(n) \tag{2.9b}$$

The equation in 2.9a has the form of a linear equation. There is a constant term $d(n)$ determining the intersect with the y-axis and $f(r, n)$ which defined the slope. The picture in 2.7 clarifies the aforementioned remarks. A higher loss exponent causes an increased offset $d(n)$ on the y-axis The same applies for the slope $f(r, n)$. A higher loss exponent n entails a steeper slope $f(r, n)$. Figure 2.8 plots the path loss for different values of the path loss exponent using linear scaling on the x-axis. Using logarithmic scaling on the x-axis yields a plot that is shown in figure 2.9.
A common problem is to calculate the maximum range $r^d_{max}B$ given the transmission power of the sender and the sensitivity of the receiver. The term sensitivity is used to denote the minimal power that is required by the receiver to ensure proper operation. This can be achieved easily by solving the equation 2.9 for the distance. Thus we can determine the maximum range for a one-way communication (forward-channel) from sender (reader) to the receiver (tag) (see figure 2.2).

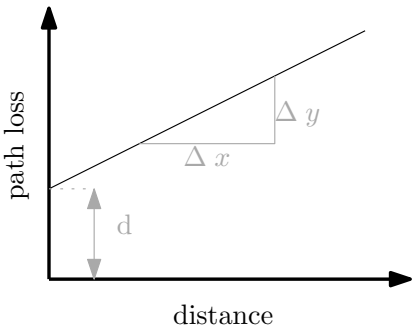


Figure 2.7: Linear equation parameterizing the log-distance path loss

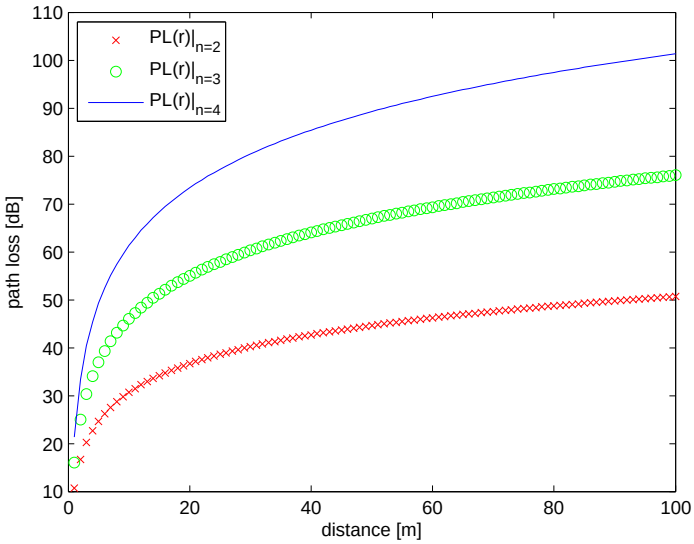


Figure 2.8: Path loss as a function of distance with linear scaling

$$r_{max}^{dB} = 10 \cdot log10\left(\frac{\lambda}{4 \cdot \pi}\right) + \frac{1}{n} \cdot \left(P_{reader}^{dB} - P_{tag}^{dB}\right) \tag{2.10}$$

The formula from 2.10 can also be applied for the backward-channel. In this scenario the role of the sender and the receiver is reversed. Given the transmission power of the sender (tag) and the sensitivity of the receiver (reader) we can compute the maximum distance for the backward-channel.

### 2.4.5 Human body model

During the last decade the rapid growth in field of physiological sensors has been a key enabler for human body area networks. A possible practical realization uses RFID as the communication technology of choice. The vicinity of the human body to the reader and the tag has a severe impact on the wireless communication between them. This application

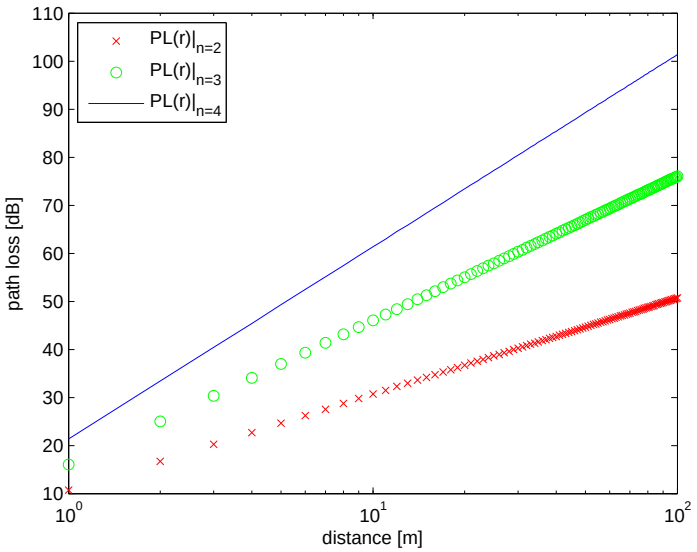


Figure 2.9: Path loss as a function of distance with logarithmic scaling

scenario requires a special model that properly fits the real-life counterpart. There is a special IEEE working group that addresses the topic of personal wireless area networks. A part of this working group (subcommittee) is just focused on the modeling of the communication channel. The paper in [7] summarizes the activities and recommendations of the channel modeling subgroup.
Assuming the validity of the superposition principle we can decompose the path loss (see equation 2.11). One part that solely depends on frequency $PL(f)$ and the other part $PL(r)$ which is a function of distance.

$$PL(f,r) = PL(f) + PL(r) \tag{2.11}$$

There are two possibilities to determine $PL(f)$. The empirical approach uses a vectored network analyzer (VNA), measuring equipment, a test subject and an anechoic chamber[4]. The measurement setup is depicted in 2.10.
Relating the input power to the output power while altering the frequency yields $PL(f)$ as suggested by [9]. Assuming that we are working with a fixed frequency we can drop the frequency dependent term. The path loss $PL(r)$ is based upon the log-distance path loss formula from 2.9.

$$PL(r) = k \cdot log10(r) + d + N \tag{2.12}$$

Where the parameters in equation 2.12 correspond to the same parameters as in section 2.4.4. The parameter $k$ defines the slope and parameter $d$ is the offset on the y-axis. Inspecting a real-life wireless communication channel we notice that its properties change depending on time, location and frequency. Since there is no clear line-of-sight between sender and receiver

[4] an echo-free room, absorbing electro-magnetic radiation

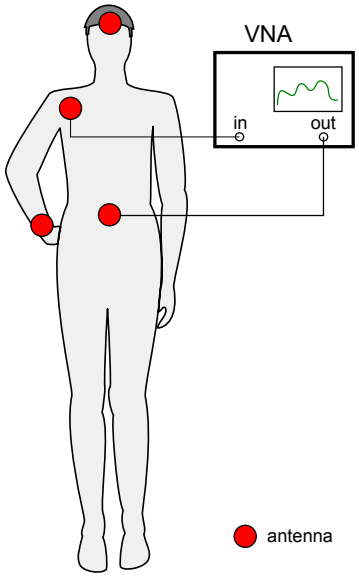


Figure 2.10: On-body measurement setup using a VNA

the transmission is distorted by the surrounding objects. By introducing a random process to the path loss formula we try to mimic this behavior. In literature this effect is often called shading. $N$ is a log-normal distribution with zero mean and the variance $\sigma$. Figure 2.11 plots the enhanced path loss formula which take into account the effect of shading. The actual parameters are taken from [7] for body surface to body surface communication using channel model CM3 at 900MHz. When using the model from [7], make sure that the distance is converted to millimeter. See appendix A.1 for details on the log-normal distribution.
An alternative approach to model the human body as a communication channel involves a model that is based on the research of [25].

## 2.5 Antenna theory at a glance

The core objective of an antenna is the conversion of a lead bounded signal into an electromagnetic wave using air as a spreading medium and vice versa. Applications usually dictate the bandwidth, center frequency etc. of an antenna. In terms of analog circuitry this behavior is similar to a resonant circuit. The basis for our further investigations are based upon a resonant circuit (see left part of figure 2.12). Starting at the left we can see a basic resonant circuit. As progressing from the left to the right the circuit is geometrically modified keeping its original properties. The rightmost part is a piece of wire that acts as antenna. The frequency dependence of an antenna can be explained by the fact that its equivalent circuit diagram is a resonance circuit.
A more complete setup using an antenna in transmission mode is depicted in figure 2.13. The signal to be transmitted is generated by the signal source on the left. The transmission line acts as a wire bound wave guide. The hopper represents the antenna and acts as the transmission zone from wire as a transmission medium to the air interface. From now on the

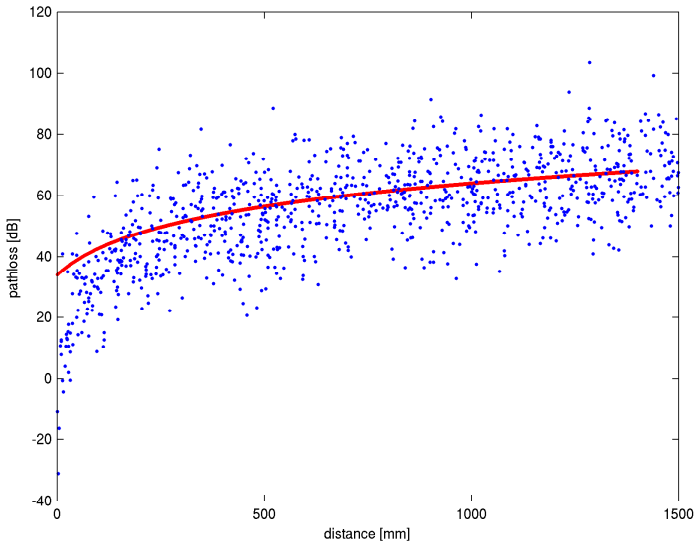


Figure 2.11: Enhanced path loss formula including shading, $a = 28.8$, $b = -23.5$, $c = 11.7dB$

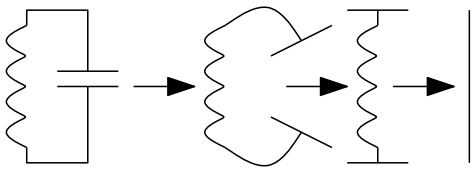

Figure 2.12: The metamorphosis of a resonant circuit into an antenna

signal is spreading as an electro-magnetic wave using air as an transmission medium.

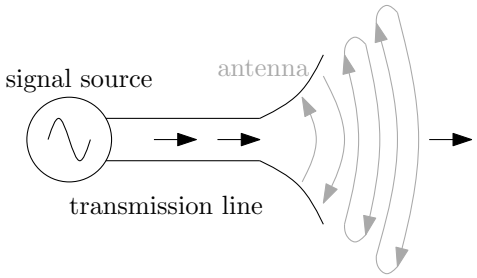


Figure 2.13: Antenna converting a lead bound signal to a wireless signal

As already mentioned an antenna works as a transducer in both directions. Due to the principle of reciprocity we can use an antenna for receiving and sending an electro-magnetic wave. The picture in 2.14 outlines the receiving scenario. As the electro-magnetic wave faces the antenna, it is picked up and fed to the receiver.

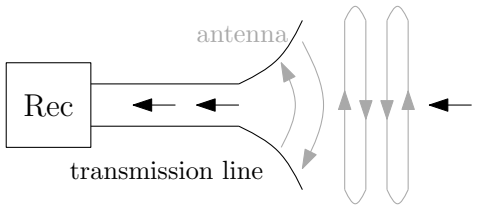


Figure 2.14: Antenna that picks up a wireless signal and converts is to a lead bound signal

### 2.5.1 Modeling of the tag

The tag itself can be further decomposed into the antenna and the tag IC. In section 2.5 we already derived the equivalent circuit diagram of an antenna. As a first approximation we represent the tag IC by a plain RC circuit. In a practical implementation of the tag IC its input impedance is not constant over time and depends on the current state of the tag. Our rudimentary model neglects a lot of details but allows efficient simulation.
Thinking back to section 2.5 we already acquired some insights on the equivalent circuit diagram of an antenna. From the source's perspective the tag IC acts as a load that is connected to the antenna terminals. The whole setup is fed by a signal source, representing the signal send from the reader. Picture 2.15 shows the simulation model of the tag.

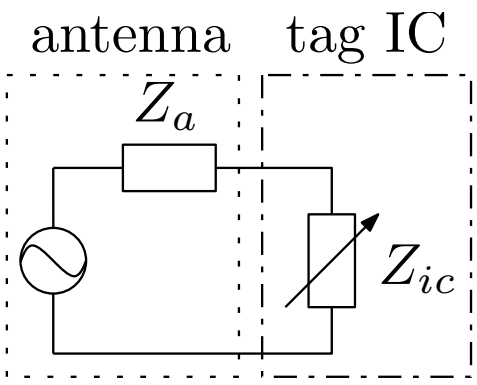


Figure 2.15: Receiving circuit modeled as impedance network

It is important to notice, that only the power delivered to the ohmic part of the antenna impedance is radiated via the air interface. A large part of this thesis is concerned about the behavioral analysis of the circuit in figure 2.15. In order to gain more insight on receiving circuit, we have to replace the impedance by their subcircuits. After this we end up with a circuit that is shown in figure 2.16.
The Friis equation provides us with the facility to calculate the power that is received at the tag. Looking at the tag equivalent circuit diagram we notice that the power at the tag IC itself depends on the impedance of the tag antenna and the tag IC. The next section elaborates on the issue of complex impedance matching between these two entities.

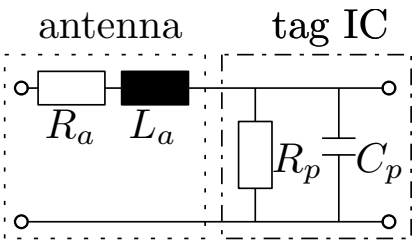


Figure 2.16: Detailed receiving circuit modeled as impedance network

### 2.5.2 Advanced Friis equation

The reply from the tag which is sent back to the reader uses the mechanism of backscattering. All the power that is dissipated at the resistor $R_a$ is re-radiated (backscattered) by the antenna (see 2.16). Modulated backscattering is achieved by the variation of the current through the resistor $R_a$. In its pimpliest form this can be achieved by short-circuiting the antenna terminals. This schema is formally described by the paper in [15]. The equation in 2.14 models the power $P_{IC}$ at the tag IC as a function of its impedance.

$$P_{IC} = P_{avail} \cdot \left(1 - \left|\frac{Z_{ic} - Z_a}{Z_{ic} + Z_a}\right|^2\right) \tag{2.13}$$

$$= P_{avail} \cdot \left(1 - \Gamma^2\right) \tag{2.14}$$

Where $P_{avail}$ is the available power that is received via the air interface which is computed via the Friis equation. With the aid of the Friis equation, we can rewrite the equation above expressing the power at the tag IC as a function of the distance, the reader transmission power and the matching at the tag side.

$$P_{IC} = P_{reader} \cdot \left(\frac{\lambda}{4 \cdot \pi \cdot r}\right)^2 \cdot \left(1 - \Gamma^2\right) \tag{2.15}$$

We should take time to interpret the formula we just derived. Assuming that the tag IC impedance $Z_{ic}$ is the complex conjugate of tag antenna impedance $Z_a$. Using this fact we can reduce the equation we derived earlier. In case of matching half of the incident power is dissipated at the tag. The remaining power is dissipated at the ohmic part of the antenna resistor.

$$\begin{aligned} P_{IC} &= P_{avail} \cdot \left(1 - \left|\frac{Z_{ic} - Z_a}{Z_{ic} + Z_a}\right|^2\right) \\ &= P_{avail} \cdot (1 - 0) \\ &= P_{avail} \end{aligned}$$

Supposing that the tag IC is shorted we can derive following formula:

$$\begin{aligned} P_{IC} &= P_{avail} \cdot \left(1 - \left|\frac{0 - Z_a}{0 + Z_a*}\right|^2\right) \\ &= P_{avail} \cdot (1 - 1) \\ &= 0 \end{aligned}$$

Due to the fact that there is a mismatch between the tag antenna and the tag IC, the power is reflected from the tag IC back to the source. As a further consequence, this power is radiated via the tag antenna. In this case no power is dissipated at the tag IC since the voltage across the antenna terminals is zero. The difference between these two cases are their different radar cross-sections. It is vital that the difference between these modulation states is as large as possible. This fact makes it easier for the tag to distinguishing the two modulation states.

### 2.5.3 Scattering parameters

The analysis of electrical networks studies the behavior of a given circuit diagram. In order to cope with the complexity of large electrical networks, we subdivide it into smaller subcircuits. These subcircuits are called two-port networks. Studying the properties of the subcircuits is often easier than the analysis of the entire network as a whole. Once we characterized all subcircuits we can cascade them to describe the entire network. By hiding the internal decomposition of each block we get rid of the calculation of the internal currents and voltages. As the subcomponent is treated as a blackbox we can calculate the output from the input using a behavioral description ignoring its internal structure.

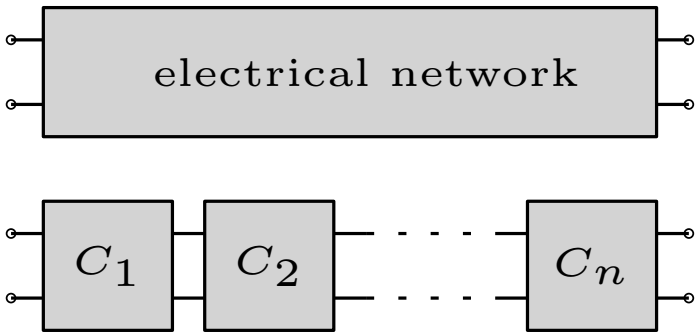


Figure 2.17: System that is decomposed into small subcircuits

From that follows that we need formalism that lets us describe the characteristics of each individual block. The theory of two-port networks offers a variety of different parameters that characterizes the system depending on the individual application. In our case we will stick to the scattering parameters that are heavily exploited in the area of radio frequency engineering. Instead of working with voltage and current the analysis is based on the power of incident and the reflected wave at the input and the output port.
Figure 2.18 depicts a two-port network that is described via scattering parameters. Parameters $a_1$ and $a_2$ are a measure of the waves that are traveling towards the systems. The parameters

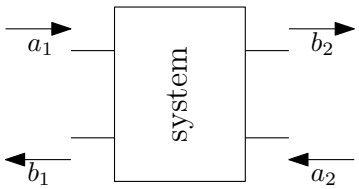


Figure 2.18: most basic building block that is described by scattering parameters

$b_1$ and $b_2$ represent the measure of the outgoing waves of the system. The equation in 2.16 defines the calculation of the scattering parameters for a given system. Due to our setup it is sufficient to restrict the derivation of the scattering parameters to a two-port network. The waves traveling towards the network are indicated via the letter a followed by an index. The same holds true for reflected waves that labeled with the letter b.

$$\begin{pmatrix} b_1 \\ b_2 \end{pmatrix} = \begin{pmatrix} S_{11} & S_{12} \\ S_{21} & S_{22} \end{pmatrix} \cdot \begin{pmatrix} a_1 \\ a_2 \end{pmatrix} \tag{2.16}$$

Instead of the matrix representation that is used in equation 2.16 we can use a system of linear equations (see equation 2.17).

$$\begin{aligned} b_1 &= S_{11} \cdot a_1 + S_{12} \cdot a_2 \\ b_2 &= S_{21} \cdot a_1 + S_{22} \cdot a_2 \end{aligned} \tag{2.17}$$

The first line of equation 2.17 is used to calculate the outgoing wave at the left port of the two-port network (see 2.18). There are two components that account for the resulting wave $b_1$. One part arises from the input wave $a_1$ that is reflected at the input port. The other part comes from the input wave $a_2$ from the right side. In order to calculate $S_{11}$ the output port is connected to the characteristic impedance. Due to that fact that the wave $a_2$ vanishes and we can determine $S_{11}$.

$$b_1 = S_{11} \cdot a_1 + S_{12} \cdot a_2|_{a_2=0} \tag{2.18a}$$

$$\rightarrow S_{11} = \frac{b_1}{a_1} \tag{2.18b}$$

Thinking back to the advanced Friis equation we remember $\Gamma$ which is a measure for the matching between the antenna and the tag IC. By carefully inspecting the definition of the scattering parameters we notice that there is a strong connection between $\Gamma$ and the $S_{11}$ parameter. Due to that fact we can conclude that the scattering parameter analysis is perfectly suited for a in-depth analysis for the matching between two given subcircuits. Recalling the advanced Friis equation from section 2.5.2 we notice the term on the right-hand side enclosed with brackets. Equation 2.19 is used to calculate the power at the tag IC, taking into account the matching between tag IC and the antenna. Due to that definition of $S_{11}$ we can rewrite the Friis equation using $S_{11}$. This offers us the possibility the analyze the matching between two circuit parts using the scattering parameter analysis.

$$\begin{aligned} P_{IC} &= P_{avail} \cdot \left(1 - |\Gamma|^2\right) \\ &= P_{avail} \cdot \left(1 - |S_{11}|^2\right) \end{aligned} \tag{2.19}$$

## 2.6 Phase-locked loop (PLL)

A PLL is a synchronization and clock recovery circuit which is often used in telecommunication systems. Low noise performance and a highly stable time basis are the foundation of a reliable digital communication system. Thus the design of a PLL can be seen as an important and challenging task. The working principle of a PLL is explained with an example taken from everyday's life. Properly tuning a guitar is essentially the same problem as synchronizing a PLL. A pitch from a tuning fork or another instrument acts as a reference signal. Assuming that the reference is correct the guitar player plucks the corresponding string on the guitar. By carefully listening to the difference in pitch of both tones he turns the tuning key for the current string altering the frequency till they both sound the same. The same idea is behind the working principle of a PLL (example taken from [5]).
In terms of control theory the setup of a PLL is a classical feedback system. Giving a reference signal it is the duty of a PLL to generate an output signal with the same frequency or a multiple compared to the input. It is necessary to make sure that their phase or frequency difference is below a given threshold level. The working principle of a PLL can be broken down to a few rudimentary building blocks (see figure 2.19). During the next paragraphs the features and tasks of each individual component will be discussed.

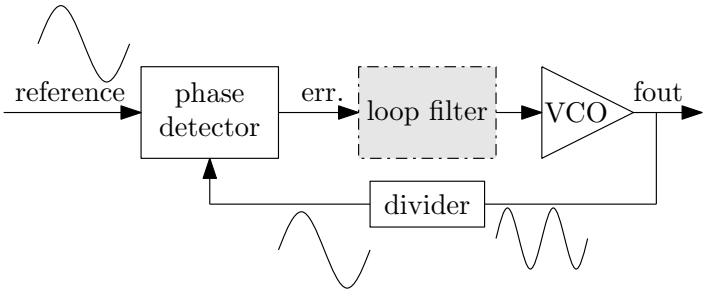


Figure 2.19: Schematic diagram of the basic PLL structure (see [3])

### 2.6.1 Phase/frequency detector

On the left-hand side is the reference signal which acts as an input to the phase/frequency detector. Whereas the output signal *"fout"* is found on the right-hand side. The first block from the left is the phase/frequency detector. Its output voltage is proportional to the phase and/or frequency difference of two given signals. We are speaking of a pll-lock to denote that the average frequency of the input signal is identical to the frequency of the output signal with a phase difference below a given value.
The working principle of a phase detector can be best described using the example of a mixer. Signal $s_1(t)$ and signal $s_2(t)$ serve as the input to the phase detector (see figure 2.20a).

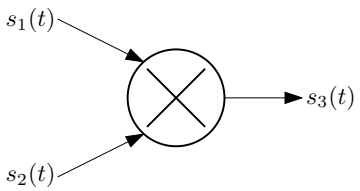


(a) Block diagram of a mixer

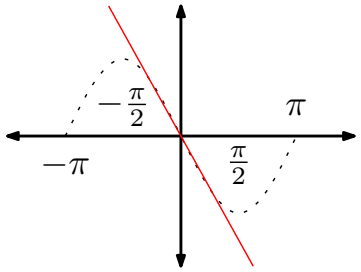


(b) Mixer based phase detector showing sinusoidal characteristics

Figure 2.20: Symbol and characteristics of phase detector based on a mixer

We assume that both signals are purely sinusoidal and have to same frequency. Their only difference is Their phasing $\Delta\varphi$. The behavior of a phase detector can be formally described with following equations:

$$s_1(t) \cdot s_2(t) = A_1 \cdot sin(2 \cdot \pi \cdot f \cdot t) \cdot A_2 \cdot sin(2 \cdot \pi \cdot f \cdot t + \Delta\phi) \tag{2.20}$$

The trigonometric identity (equation 2.21) can be used to rewrite the equation 2.20.

$$sin(x_1) \cdot cos(x_2) = \frac{1}{2}\left[sin(x_1 + x_2) + sin(x_1 - x_2)\right] \tag{2.21}$$

Inserting equation 2.21 into equation 2.20 we derive following expression:

$$\begin{aligned} s_1(t) \cdot s_2(t) =& \frac{A_1 \cdot A_2}{2}\left[sin(2 \cdot \pi \cdot f \cdot t + 2 \cdot \pi \cdot f \cdot t) + sin(2 \cdot \pi \cdot f \cdot t - 2 \cdot \pi \cdot f \cdot t + \Delta\phi)\right] \\ & \frac{A_1 \cdot A_2}{2}\left[\underbrace{sin(4 \cdot \pi \cdot f \cdot t)}_{I} + \underbrace{sin(\Delta\phi)}_{II}\right] \\ \approx & \frac{A_1 \cdot A_2}{2}\left[sin(4 \cdot \pi \cdot f \cdot t) + \Delta\phi\right] \end{aligned} \tag{2.22a}$$

Inspecting equation 2.22a we notice that we end up with two terms. The first sinusoidal term $I$ does not depend on the phasing of $s_1(t)$ or $s_2(t)$ at all. What we notice is, that the initial frequency has doubled. The argument of term $II$ is solely depending on the phasing between $s_1(t)$ and $s_2(t)$. Figure 2.20b plots the signal curve of term $II$ while changing the phasing. For a phasing between $-\frac{\pi}{2}$ and $\frac{\pi}{2}$ the sinusoidal graph can be approximated by a linear equation. As soon as the phasing is greater than $|\frac{\pi}{2}|$ we see that the error of the linear approximation increases dramatically. Assuming the phasing is reasonably small (linear region) we still have to suppress term $I$ from equation 2.22a. This is where the loop filter comes into play, which is the topic of the next section.

### 2.6.2 Loop filter

Choosing a proper loop filter structure and it's parametrization is an important design step. The boundary conditions that are given by the individual applications dictate the

PLL properties. Section 2.6.1 (mixer as phase comperator) underlines the need to suppress unwanted signal components that are introduced by the detector. The loop filter is decisive for the loop dynamic including stability, the achievable locking-range and the time it takes for the PLL to lock. Since the loop filter are low pass filters the PLL is able compensates for noisy input signals (signal recovery).
When choosing the proper bandwidth of the loop filter one has to consider following facts. A input signal that severely suffers from jitter calls for a low bandwidth loop filter resulting into a low jitter output signal. Apart from that is another term that influences the jitter of the generated output signal. The jitter of the output signal is influenced by the internal circuitry of the PLL itself. The impact of this fact is increased as the bandwidth of the loop filter is held small. Whereas a decreased loop filter bandwidth weakens the influence of the jitter from the input to the output, it increases the amount of jitter that is coming from the PLL . One has to make sure that the filter bandwidth is small enough to damp the input jitter, but making sure that the filter bandwidth is wide enough to minimize the output jitter that arises from the PLL loop.

### 2.6.3 Voltage controlled oscillator

A VCO is the umbrella term for an electronic circuit, that consists of an controllable oscillator. The voltage level at the input of the VCO determines the frequency of the periodic signal at the output. The output signal is linearly depended on the voltage level of the input signal. Figure 2.21 depicts the frequency of the output signal as a function of the input voltage. In the idealized case the VCO can be described through a linear equation that is depending on two parameters. There is the offset on the y-axis and the slope. The formal connection between the input and the output is expressed in equation 2.23.

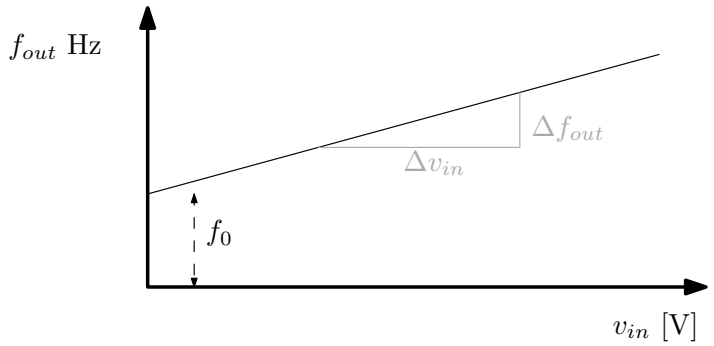


Figure 2.21: Characteristics of an idealized VCO

$$f_{out}(v_{in}) = f_0 + k \cdot v_{in} = f_0 + \frac{\Delta f_{out}}{\Delta v_{in}} \cdot v_{in} \tag{2.23}$$

When using a VCO as a building block of a PLL we have to make sure that the frequency $f_0$ is situated near the frequency of the reference signal. If the frequency span of the VCO does not include the reference frequency the lock conditions are not met. Originally we assumed that the frequency of the reference signal is the same as the frequency of the output signal.

With the use of a frequency divider in the feedback loop we can increase the output frequency by reciprocal of the divide ratio. The next section gives a short introduction to feedback dividers.

### 2.6.4 Feedback divider

An optional feedback divider can be placed into the feedback loop of the PLL. As the frequency of the feedback signal is decreased with the feedback divider we meanwhile increase the frequency of the output signal. A feedback divider offers us the possibility to cover a wider range of output frequencies.

# 3 Application study

This section is concerned about the analysis of the factors that limit the read range of a RFID UHF communication. A semi-passive RFID tag in different environments is discussed in respect to it's link budget. The Friis equation from section 2.6 is most important when calculating the loss across a wireless link. In the most simple case we need at least three parameters to draw a diagram of the link budget for a given communication scenario.
The maximum permitted transmission power of an RFID reader in Europe is given through the ETSI . Deciding if the power of the RFID reader signal is properly received at the tag, requires the parameter that defines the receiving sensitivity of the transponder. The same holds true for the reader side. There is a minimum required power level at the reader which assures, that the reply of the tag is properly received. This concludes the parameters that we need for further analysis.

## 3.1 Maximum read range for semi-passive scenario

We already know from section 2 that a semi-passive tag is known for it's outstanding receiving sensitivity. This is achieved with a battery that powers the receiving circuit of the transponder. The increased complexity of a semi-passive tag results into higher manufacturing costs. The current setup tries to achieve the maximum possible read distance. We assume that the wireless communication uses free space as propagation medium. The maximum possible transmission power of the reader is 35.16 dBm. A semi-passive tag achieves a receiving sensitivity of $-35$ dBm. The RFID reader has a receiving sensitivity of $-90$ dBm. Figure 3.1 represents the system setup for the semi-passive communication scenario.

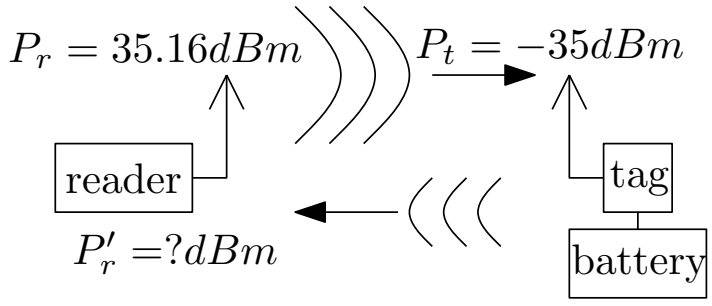


Figure 3.1: Semi-passive system architecture

Using the formula for the log-distance path loss in combination with the parameters from above we can calculate the maximum distance $r_{max}$ in equation 3.1.

$$\begin{aligned} r^{dBm} &= 10 \cdot log10 \left(1000 \cdot \frac{\lambda}{4 \cdot \pi}\right) + \frac{1}{2} \cdot \left(P_r^{dBm} - P_t^{dBm}\right) \\ &\approx 10 \cdot log10 \left(1000 \cdot \frac{0.346}{4 \cdot \pi}\right) + \frac{1}{2} \cdot (35.16\, dBm - (-35\, dBm)) \\ &\approx 14.4\, dBm + 35.08\, dBm = 49.48\, dBm \rightarrow 88.72\, m \end{aligned} \tag{3.1}$$

The calculation in 3.1 was performed for the wireless transmission from the reader to the tag. Assuming that the path loss stays the same for the transmission from the tag to the reader, we can calculate the power level at the reader (see equation 3.2). Where $PL_{fc}$ denotes the loss across the wireless link from reader to tag (forward-channel). $PL_{bc}$ is analogously used for the loss introduced by the backward-channel.

$$\begin{aligned} P_r' &= P_r - PL_{fc} - PL_{bc} \\ &= P_r - 2 \cdot PL_{fc} \\ &= 35.16\, dBm - 2 \cdot (35.16\, dBm - (-35\, dBm) \\ &= -105.16\, dBm \end{aligned} \tag{3.2}$$

We can use the values we have calculated before to draw a visual representation of the power levels. Figure 3.2 depicts the link budget for the semi-passive communication scenario.

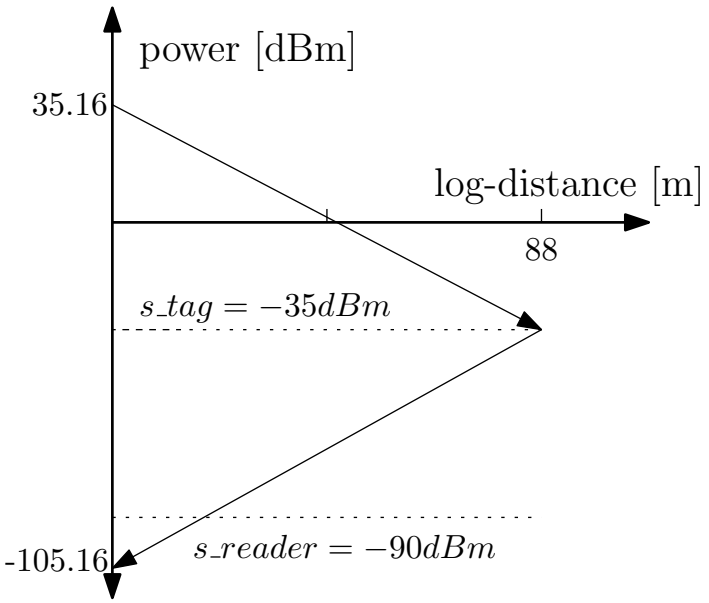


Figure 3.2: Semi-passive communication scenario aiming for maximum read range

By carefully inspecting figure 3.2 we notice that the power level of the tags reply is below the sensitivity of the reader. In this case the reader is able to talk to the tag. The reply of the tag on the other hand is not properly received by the reader. We notice that we need a mechanism at the tag that increases the power level. This is where active backscattering can be used to establish a two-way communication between reader and tag. Equation 3.3 calculates the minimum required gain at the tag.

$$gain = |P'_r - s_{reader}| = |-105.16\,dBm - (-90\,dBm)| = |-15.15\,dBm| = 15.15\,dBm \quad (3.3)$$

Figure 3.3 shows the influence of the active backscattering concept on the power link budget.

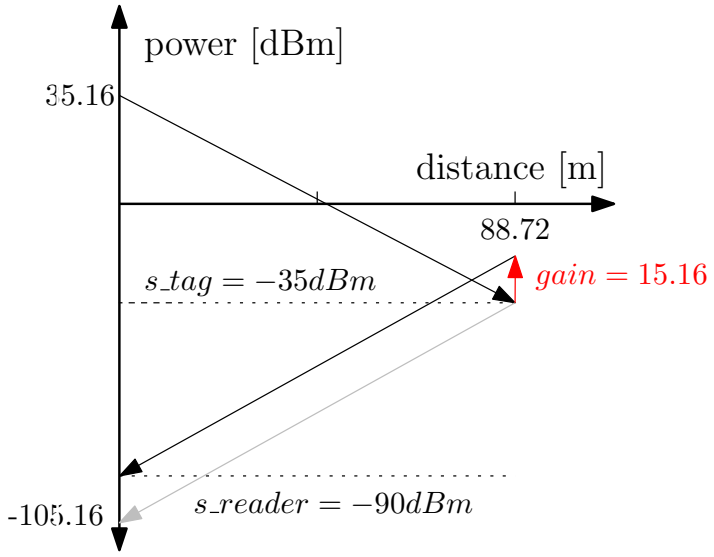


Figure 3.3: Semi-passive scenario with active backscattering at the tag

## 3.2 Human body area network

Human body area network can be seen as special application scenario of the RFID technology. To use the RFID technology in medical sector requires us to fulfil the given requirements. Electro-magnetic radiation near the human body underlies strict regulations. For example the maximum allowed reader power is much lower than the usual permitted power as given by the ETSI (see [12]). The communication scenario in figure 3.4 depicts the link budget that experiences reduced reader power. It highlights the use of the active backscattering concept in such an environment.

Figure 3.4a depicts a successful two-way communication between reader and tag. In this case we assume, that the distance between the two communicating parties is two meters. We notice that the power level received at the tag is above the minimum required boundary $s_{tag}$. What we also note is the power level of the tags reply, which perfectly achieves the minimum power at the reader.

The figure to the right (3.4b) shows the impact of decreased reader power. Reducing the reader power manifests as downwards shifts of the arrows. This shift is denoted by the small arrow at the top, reaching from point $P_1$ to $P_2$. The gray arrows denote the link budget from figure 3.4a.

Inspecting figure 3.4c we see that the received power at the reader is below its threshold level. This hinders a two-way communication since the minimum required power level is not met.

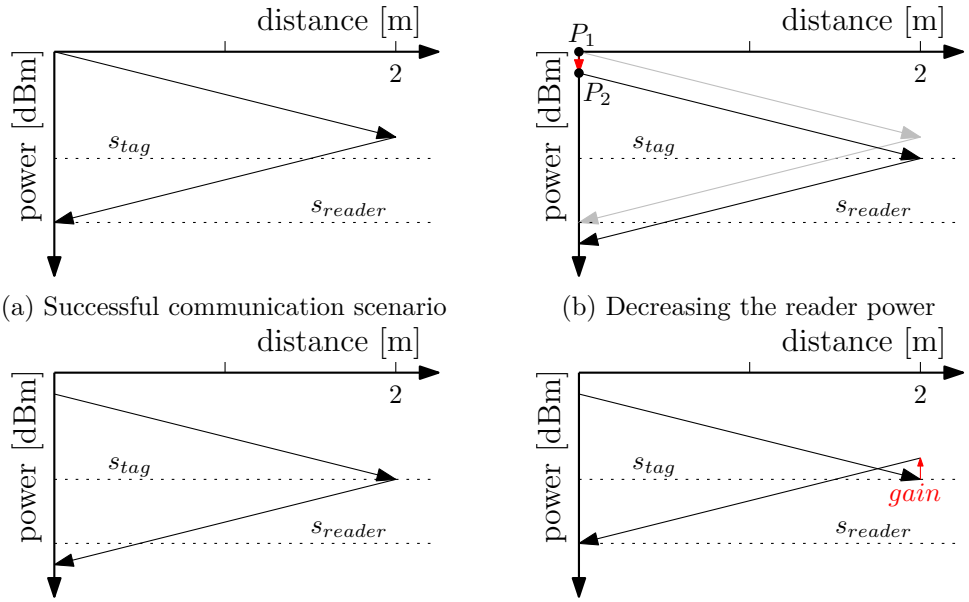


(a) Successful communication scenario

(b) Decreasing the reader power

(c) Power at the receiver is below the sensitivity level

(d) Amplifying the signal level at the tag enables a two-way communication

Figure 3.4: Human body area network power budget diagram decreasing the reader power

Knowing the path loss that is introduced by our communication channel we can use this to calculate minimum required power level at the tag that is still above the sensitivity of the reader. Figure 3.4d illustrates this procedure. We clearly see the gap between the black arrows. This gap is filled by amplifying the signal before it is backscattered towards the reader.

# 4 Link budget simulations

The main focus of this section is the simulation of operating parameters of the tag and the reader. Our investigations are based on the model we derived in section 2.5.1. Furthermore we assume that the characteristics of the tag are static and stay constant over time. Assuming free space as propagation medium we can safely use the Friis equation. This section uses a refined model of the tag. The tag antenna and the tag IC are both modeled as a complex impedance. The special form of the Friis equation from section 2.5.2 takes into account the matching between the tag antenna and the chip impedance. The impedance of the antenna is obtained with the help of the numerical simulation software ANYSYS HFSS (see [11]). Whereas the impedance of simple antennas is usually expressed in the form of a mathematical formula. Determining these impedance of the tag IC requires a special measurement setup. With this in mind we turn towards the impedance of the antenna. Maximizing the power transfer from the antenna to the tag IC requires us to attain resonance. In other words this means that the signal source sees a pure ohmic load that is obtained through the cancellation of the imaginary parts from the tag IC and the antenna.

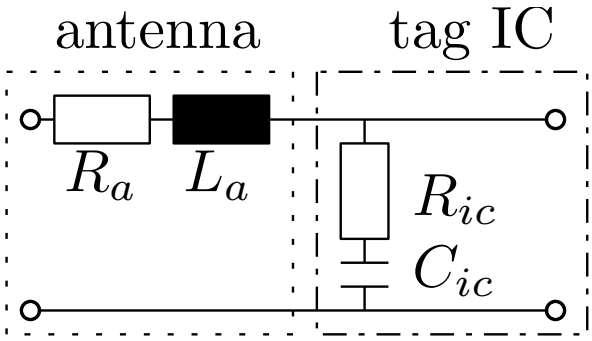


Figure 4.1: Receiving circuit modeling the tag, $R_{ic} = 23\,\Omega$ and $C_{ic} = 300\,fF$

The antenna impedance of the circuit in figure 4.1 is calculated in equation 4.1. Equation 4.1 makes use of the fact that we mentioned earlier. Applying the circumstance that the imaginary part vanishes we can calculate the missing value of antenna's inductivity. Assuming an operating frequency of 866 MHz we get:

$$Z = \Re + j\Im = R_a + R_{ic} + j\underbrace{(X_l - X_c)}_{=0} \tag{4.1}$$

$$\rightarrow X_l - X_c = 0 = \omega \cdot L_a - \frac{1}{\omega \cdot C_{ic}} \tag{4.2}$$

$$= 2 \cdot \pi \cdot f_c \cdot L_a = \frac{1}{2 \cdot \pi \cdot f_c \cdot C_{ic}} \tag{4.3}$$

$$\rightarrow L_a = \frac{1}{(2 \cdot \pi \cdot f_c)^2 \cdot C_{ic}} = 112.59\,nH \tag{4.4}$$

Having calculated all missing parameters we assume that the tag antenna is fixed and its electrical characteristics are known. The tag IC which is connected to the antenna terminals represents the load. The simulation takes into account different types of tag IC realizations which is reflected by different characteristic impedances. Whereas the tag antenna impedance is held constant during the entire simulation scenario the tag IC changes depending on its realization. In our case the spectrum of different tag ICs is spanned by a variety of different rectifier realization that are found in the RF front-end of the tag IC. Table 4.1 summarizes the parameters for the different types of rectifiers.

| type | $R_p$ | $C_p$ |
|---|---|---|
| CTS | 37000 Ω | 300 fF |
| UHF1 | 9400 Ω | 300 fF |
| UHF2 | 3000 Ω | 300 fF |
| UHF3 | 25000 Ω | 300 fF |

Table 4.1: Parameters of the different rectifier realizations

Table 4.1 assumes a different topology for the impedance that represents the tag IC. Instead of a series circuit of a resistor and a capacitor a parallel circuit is used. Figure 4.2 depicts the tag IC that is represented by the parallel RC circuit.

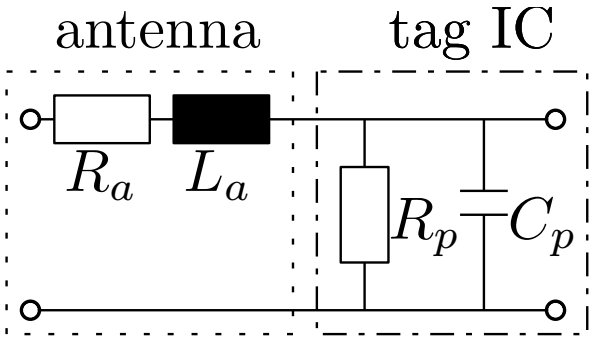


Figure 4.2: Receiving circuit modeling the tag IC in parallel RC topology

Our preceding considerations assumed that the load is a series RC circuit. This means that we have to convert the load topology to a parallel circuit. That includes the calculation of the

required values of the parallel RC circuit. Appendix A.3 is concerned with the shunt-series transformation of a 2-port network in general. For details about the derivation see the afore-mentioned section of the appendix. The outcome of this appendix serves as a basis for our further investigations. If we assume that the impedance of the antenna is fixed, we can calculate the values for the tag IC which is represented by an RC parallel circuit.

$$Q = \frac{X_s}{R_s} = \frac{2 \cdot \pi \cdot f \cdot L}{23\,\Omega} = \frac{2 \cdot \pi \cdot 866\,MHz \cdot 112.59\,nH}{23\,\Omega}$$
$$= \frac{612.47\,\Omega}{23\,\Omega} = 26.63$$

$$R_p = R_s(1 + Q^2) = 23(1 + 26.63^2) = 16332.32\,\Omega \tag{4.5}$$

$$X_p = X_s(1 + Q^{-2}) = X_s(1 + 1.41 \cdot 10^{-3}) \approx X_s \tag{4.6}$$

$R_p$, calculated via equation 4.5, represents the ideal resistance in the sense of power transfer. This fact is supported by the simulation that variates the resistor $R_p$. Calculating the capacity $C_p$ is carried out using equation 4.6. Due to the high magnitude of the quality factor $Q$ it can be simply neglected.
The solid line in figure 4.3 shows the progress of the factor scaling the Friis equation. We notice that this factor approaches one, as soon as $R_p$ is within the vicinity of the value calculated in equation 4.5. The circles represent the discrete values in table 4.1.

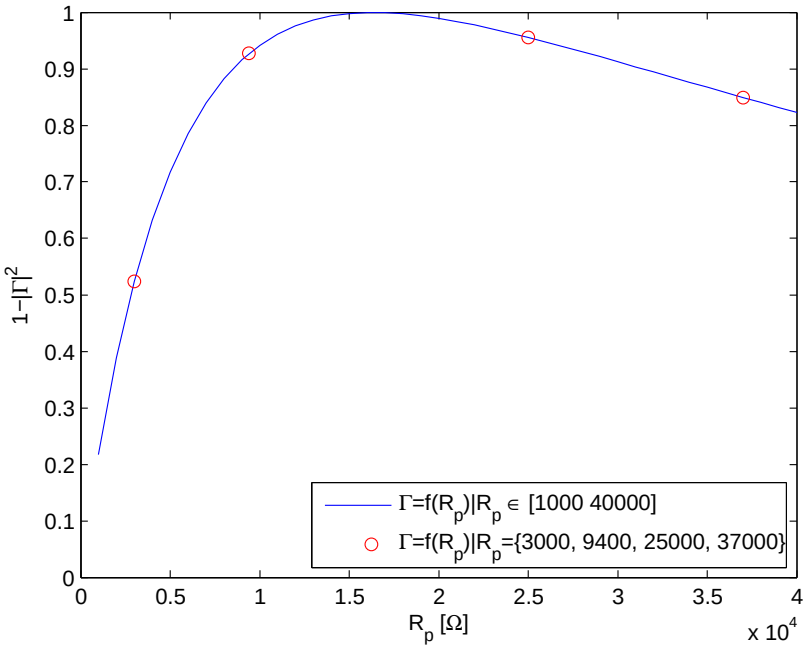


Figure 4.3: Damping factor of the Advanced Friis equation as a function of $R_p$

Since all required parameters are known in advance, we can calculate $\Gamma$ for each individual tag IC. We utilize the antenna impedance as calculated in equation 4.1 to determine each

individual Γ as stated in table 4.1. Inspecting the advanced Friis equation in 2.14 we notice, that it is reduced to its basic form for Γ close to zero. For small values of Γ we assume that the impedance of the antenna and the tag are matched. Equation in 4.7 singles out the rightmost term of the advanced Friis equation. Using the values from table 4.1 we can calculate the scaling factor (see equation 4.7).

$$1 - |\Gamma_i|^2 = 1 - \left| \frac{Z_{ic}^i - Z_a}{Z_{ic}^i + Z_a} \right|^2 \tag{4.7}$$

$$1 - |\Gamma_{CTS}|^2 = 0.5420 \tag{4.8}$$
$$1 - |\Gamma_{UHF1}|^2 = 0.9556 \tag{4.9}$$
$$1 - |\Gamma_{UHF2}|^2 = 0.8494 \tag{4.10}$$
$$1 - |\Gamma_{UHF3}|^2 = 0.9271 \tag{4.11}$$
$$\tag{4.12}$$

In terms of logarithmic domain the scaling factor is noticeable as an additive term. The plots in figure 4.4 and figure 4.5 show the power received at the tag as a function of the distance for the values given in equation 4.8. The individual signal traces of the logarithmic plot differ from each other just by the offset on the y-axis. This offset is just the logarithmic difference in their distinct Γ.

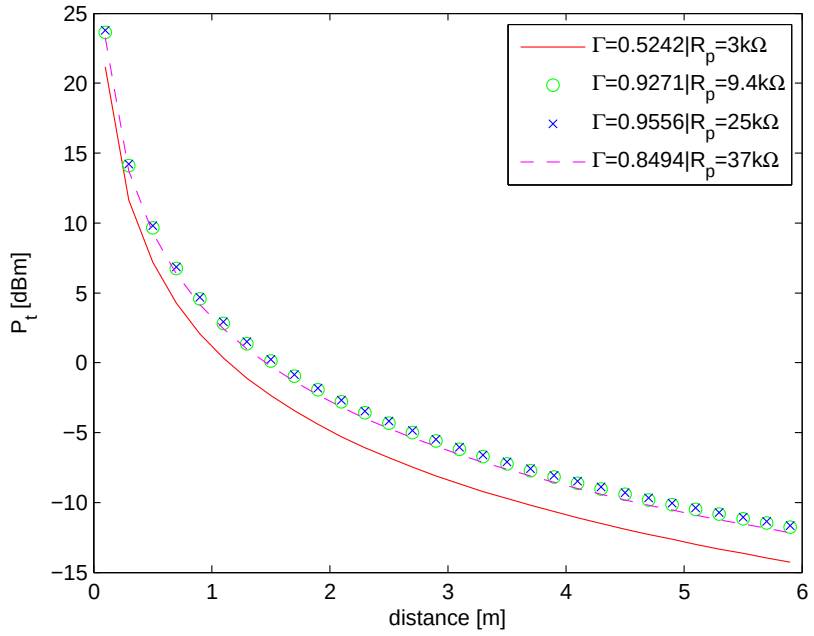


Figure 4.4: Received power as a function of the distance (linear scale)

Another approach combines the above mentioned simulations varying the distance and the load resistor $R_p$. The new simulation varies the distance simultaneously with the resistor $R_p$

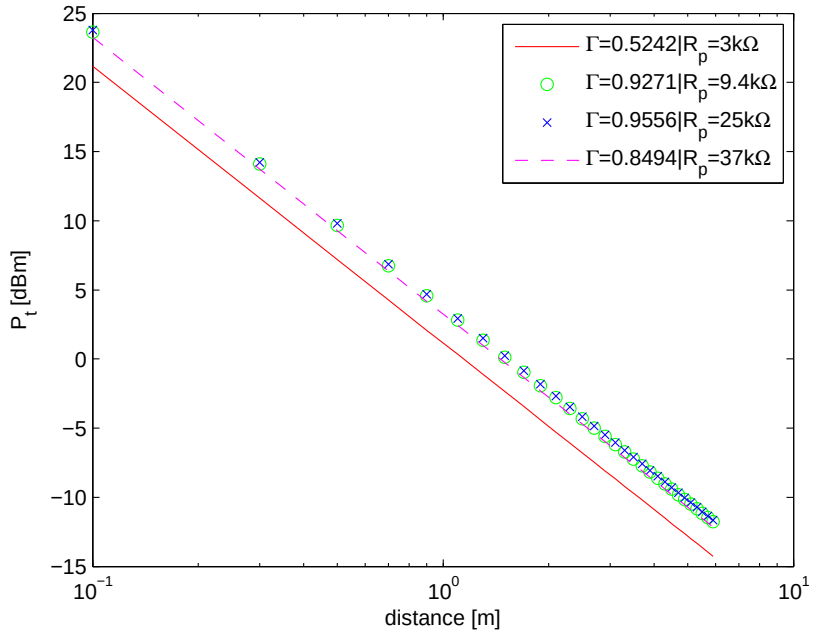


Figure 4.5: Received power as a function of the distance (logarithmic scale)

while calculating the received power. Modifying two variables at the same time effectively spans a 2-D space. Calculating the received power that is represented by the simulation parameters yields a surface plot. Figure 4.6 depicts the outcome of the afore mentioned simulation. We already investigated the power simulation with variable distance. As seen before, the received power decreases by the square of the distance. We also notice the influence of the resistor $R_p$ on the received power. As the power level is heavily influenced by the distance we notice a large dynamic domain. From the plot we can see, that a small variation of distance has a huge impact on the received power level. Whereas the load resistance has an inferior influence. Due to that reason the impact of a variable resistor $R_p$ on the received power is not obvious.
In the case of the surface plot the tag sensitivity is represented by a plane in the xy-axis. The distance of the value of the resistor $R_p$ causing the power to drop below the sensitivity plane which means that the reader is not able to successfully contact the receiver. Due to the reason of readability we omitted this plane in figure 4.6.

## 4.1 Human body area network

In contrast to the simulation scenario from the previous section we are faced with a different environment that dictates other boundary conditions. Having in mind the application scenario from chapter 2.4.5 we recall the architecture of the human body area network. A reader is placed right in the center of the human body. Sensors are then placed on the human body recording its vital signs. For our further investigation it is assumed that the human body does not move during the recording of the human vital signs. This prerequisite offers us the

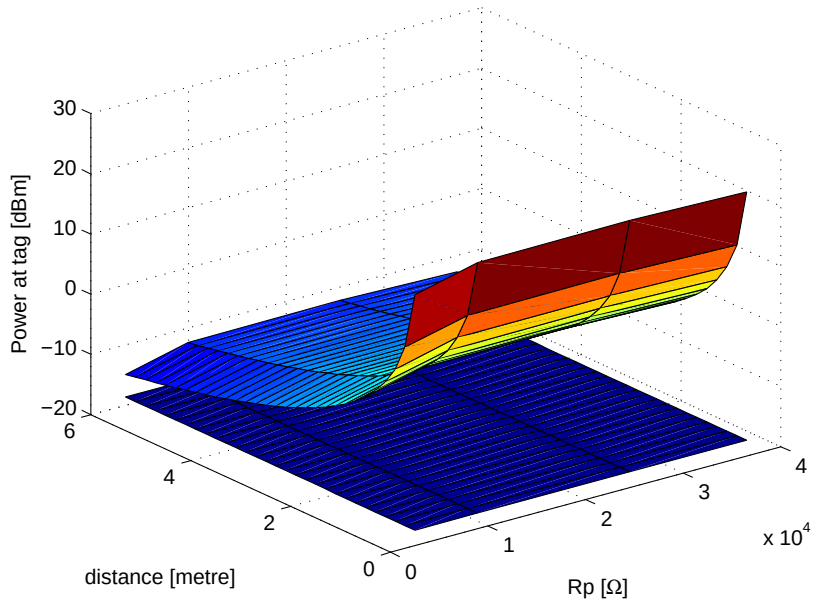


Figure 4.6: Power at the tag as a function of distance and $R_p$

possibility to safely assume that the distance between the reader and the tag is constant. In contrast to the preceding simulation we now assume a fixed distance of one meter. This simulation is focused on the transmission power of the reader instead of the maximum read range. In this scenario we vary the transmission power of the reader and observe its influence on the tag. The area of application in the field of human body area networks require the reader to be attached to moving patients. This can only be achieved by a battery-powered reader. Therefore we have to ensure that the reader is operated in an energy efficient way. In our case we are trying to achieved that by decreasing the reader power to a minimum, still enabling a two way communication. In this scenario the maximum permitted transmission power is much lower than usual, having a positive effect on the overall power consumption. Instead of monitoring the power at the receiving side of the tag we are now focusing on the voltage at the antenna terminals. The Friis equation yields the power that is delivered to the receiving circuit as a whole. Beginning with the received power at the tag we can deduce the voltage that ends up at the tag IC. Recalling the figure 2.15 from the introduction we already discussed the components of the receiving circuit. This model serves as a starting point for the derivation of the voltage $U_t$ at the tag IC. Figure 4.7 clarifies the architecture of the receiver indicating the current $I$ and the terminal voltage $U_t$.
The power dissipated at the receiving circuit is calculated below:

$$P_{tag} = I^2 \cdot Z = I^2 \cdot (Z_a + Z_{ic}) =$$
$$\rightarrow I = \sqrt{\frac{P_{tag}}{Z}}$$

Having calculated the current we can compute the voltage at the tag IC as shown in equation

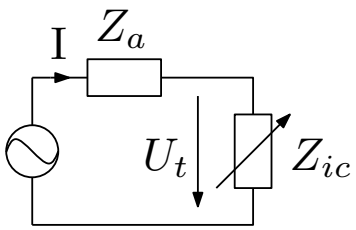


Figure 4.7: Power at the tag as a function of distance and $R_p$

4.13.

$$U_t = I \cdot Z_{ic} = \sqrt{\frac{P_{tag}}{Z}} \cdot Z_{ic} = \sqrt{\frac{P_{tag}}{Z_a + Z_{ic}}} \cdot Z_{ic} \tag{4.13}$$

The calculated power received at the tag is a real valued quantity. Since the voltage $U_t$ depends on the impedance $Z$ we obtain a complex valued result.

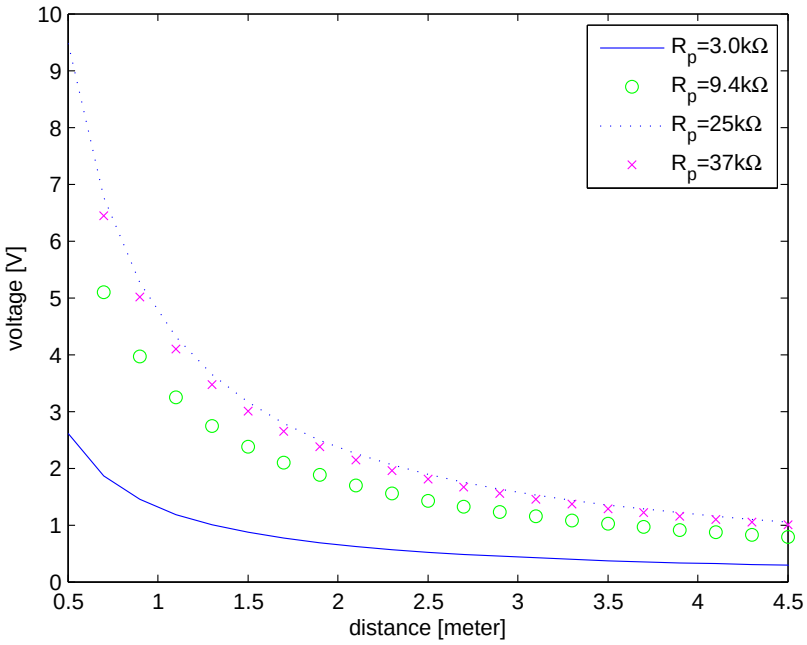


Figure 4.8: Voltage at the tag as a function of distance and $R_p$

The different traces in figure 4.8 represent individual values of resistor $R_p$. For values situated around 16.332 kΩ we notice a maximum of the received voltage. In the vicinity of the reader (near-field conditions for $distance < 0.312\,m$) the received voltage exceeds the range of typical values. This fact originates from the circumstance that our setup assumes idealized surrounding with no losses. In a real setup the typical reading of the received voltage is much lower. We also notice the exponential decrease of the voltage analogously to the trend of the

received power as the distance between sender and receiver is increased.
Another approach is focused on the voltage $U_t$ and the current $I$ as a function of the resistor $R_p$. Logarithmic scaling of the x-axis allows a clear representation of $U_t$ and $I$ over a wide range of values. As in the simulation scenario from before we assume that the received power is constant. The effective power that is delivered to the tag IC is a function of the resistor $R_p$. With the help of the attenuating factor originating from the advanced Friis equation we can calculate the effective power. Inspecting figure 4.9 we clearly notice that a maximum of the current and voltage is attained as we achieve matching. The outcome of the simulation backups the value for resistor $R_p$, that was already obtained from calculations and previous simulations.

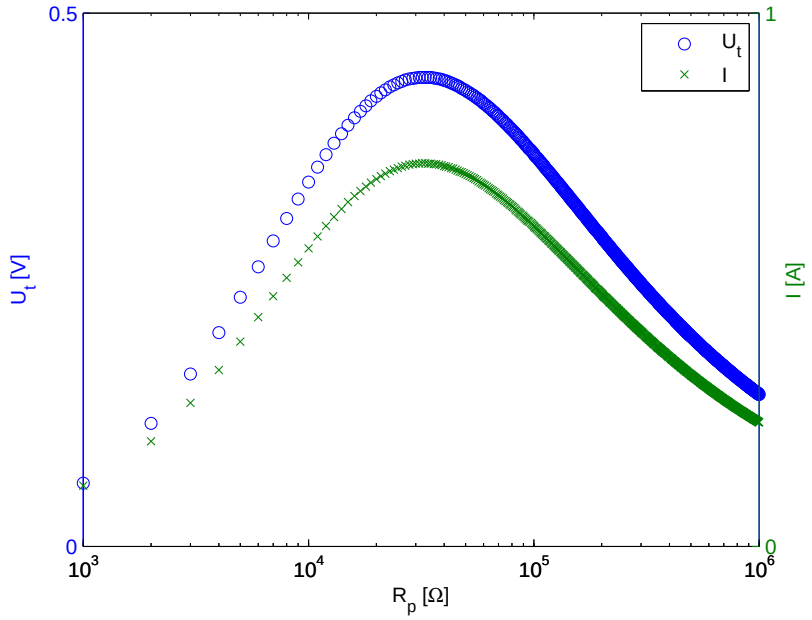


Figure 4.9: Voltage $U_t$ and current $I$ as a function of $R_p$ on logarithmic scale

## 4.2 Minimum operating voltage at the transponder

In this setup we are using a different approach. Instead of starting our investigation on the reader-side, we will now start our analysis on the tag-side. Thinking back to section 2.5.1 we can recall the internal structure of the tag IC. Each individual circuit part requires a minimal voltage supply to ensure proper operation. Our further investigations favor the digital part to underline the need for a minimal operating voltage.
An inverter can be seen as the most basic CMOS circuit, serving as the basis for further reasoning. Figure 4.10 shows the circuit diagram of an inverter. In the most simple case a transistor can be seen as the equivalent of a switch that is controlled via the input voltage. A transistor that is modeled as a switch has two states, being either closed or opened. Depending on the transistor type the switch is either closed or opened if voltage level at the gate. As

soon as the input voltage exceeds the threshold voltage of the transistor located at the bottom of the figure, the output port is shorted to ground.
Assuming the received power at the tag results into a voltage below the threshold voltage of a transistor, we realized that we cannot drive any CMOS logic at all. As soon as the voltage exceeds the threshold voltage, we can influence the output state. Alternating the output voltage causes a current that either charges or discharges the load capacitor at the output. Due to the fact that the application dictates a tight timing margin, we have to make sure that this state transition is accomplished within a given time interval. For input voltage twice the threshold voltage we assume that this requirement can be met.

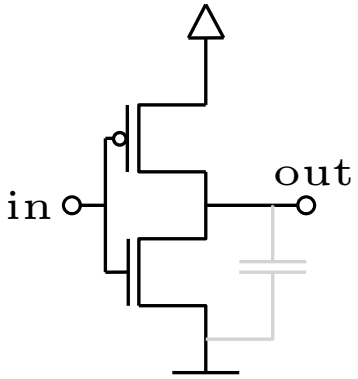


Figure 4.10: A CMOS inverter: the most basic CMOS circuit

As before mentioned we assume a minimum required voltage $U_t$ at the tag IC. This serves as a starting point to derive the power that has to be delivered to the tag in order to attain proper operation. Similar to the calculation in section 4.1 we can derive the minimum required power level.

$$P'_{tag} = U \cdot I = Z \cdot I^2 = Z \cdot \left(\frac{U_t}{Z_{ic}}\right)^2 \tag{4.14}$$

Where $P'_{tag}$ is the effective power that is dissipated at the tag taking into account the matching between the antenna and the tag IC.

$$\begin{aligned} P'_{tag} =& P_{tag} \cdot (1 - |\Gamma|^2) \\ \rightarrow P_{tag} =& \frac{P'_{tag}}{1 - |\Gamma|^2} = \frac{Z \cdot \left(\frac{U_t}{Z_{ic}}\right)^2}{1 - \left|\frac{Z_{ic} - Z_a}{Z_{ic} + Z_a}\right|^2} \end{aligned} \tag{4.15}$$

The next step involves calculating the required power at the reader-side using the path loss equation. Assuming a fixed distance and free space as the propagation medium we can use the Friis equation to calculate the transmission power of the reader.

$$P_{reader} = P_{tag} \cdot \left(\frac{4 \cdot \pi \cdot r}{\lambda}\right)^2 \tag{4.16}$$

Taking the rightmost term from equation 4.15 and substituting it into equation 4.16 we get:

$$P_{reader} = \frac{Z \cdot \left(\frac{U_t}{Z_{ic}}\right)^2}{1 - \left|\frac{Z_{ic} - Z_a}{Z_{ic} + Z_a}\right|^2} \cdot \left(\frac{4 \cdot \pi \cdot r}{\lambda}\right)^2 \tag{4.17}$$

With equation 4.17 we can calculate the minimum power at the reader-side ending up with the minimum required voltage at the tag. The minimum required voltage is 1 V at a distance of 1 m. Using the impedances from table 4.1, we can calculate the signal transmission power at the reader for all rectifier realizations.

| $R_p$ | $P_{reader}$ | $P_{reader}$ |
|---|---|---|
| $k\Omega$ | $\mu W$ | $dBm$ |
| 37.0 | 2.7 | 31.98 |
| 9.4 | 10.6 | 34.38 |
| 3.0 | 33.3 | 40.53 |
| 2.5 | 4.0 | 32.06 |

Table 4.2: Minimum transmission power at the distance of 1 m assuming 1 V at the receiver

# 5 Optimization of Antenna to tag IC matching

We have learned from the last section that the matching between antenna and tag IC is decisive for the amount of power that is delivered to the tag IC. One way of increasing the power at the tag IC is focused on the matching optimization between antenna and tag. The figure in 5.1a depicts the equivalent circuit diagram of the tag. The definition of matching implies that the circuit can be seen as a purely restive load. This is achieved through the cancellation of capacitive and inductive circuit components.
Figure 5.1 shows the circuit diagram of the tag, wheres the left part (figure 5.1a) uses a more general form to represent the characteristics of the tag. The right part (figure 5.1b) shows the internal decomposition of the antenna and the tag IC impedance. Achieving the state of matching requires us to understand the circuitry behind the generic impedance. The input impedance of the tag IC is crucial for the designing the tag antenna. In common practice the tag antenna is realized to compensate the imaginary part of the tag IC. The paper in [16] is concerned with the design of a tag antenna matching the corresponding tag IC. During the course of this chapter we assume that the design of the tag antenna is fixed. We focus on different rectifier realization that are used within a static antenna design. It is evident that this leads to an impedance mismatch between antenna and tag. By introducing concept of a matching circuit, we try to compensate for that fact.
Figure 5.2 is based on the already known circuit topology that was discussed earlier. We notice the new block labeled with *matching*. The purpose of this block is to convert the impedance between the right and left part of the transponder circuit. By using the divided and conquer approach, we split the circuit in two parts. The left part consist of the antenna impedance and the right part comprises the antenna impedance. As a first step we are matching the antenna impedance to the load of $50\,\Omega$. Figure 5.3a depicts the resulting circuit diagram. By applying the same procedure on the right part of the circuit we obtain the circuit shown in figure 5.3b. What's left to do is the combination of the two approaches

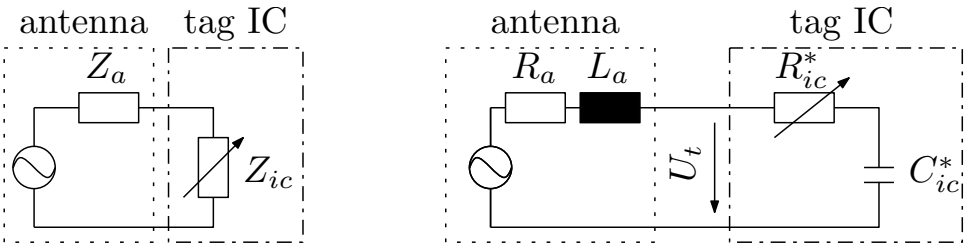


(a) Equivalent circuit diagram of the tag (b) Detailed circuit diagram of the tag

Figure 5.1: Equivalent circuit diagram of the transponder

yielding a single matching circuit.

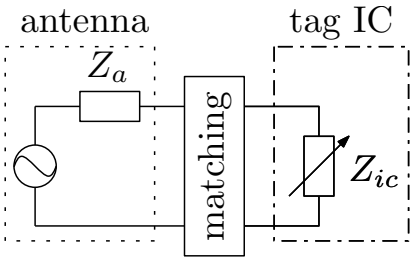


Figure 5.2: Receiving circuit with additional matching block

## 5.1 Matching the tag antenna

This task is accomplished with the help of a smith chart. There is a software tool in called *smith.exe*[8] which helps us designing the matching circuit. By entering the operating frequency and the impedance we can graphically solve our matching problem. The outcome is the topology and parametrization of the matching circuit.
The smith chart in figure 5.4 depicts the case of tag antenna impedance matching. The point *DP1* represent the impedance of tag antenna. Inductive loads can be found in the upper half of the smith chart. The center of the circle represent the characteristic impedance. By adding two passive components we try to move *DP1* to the center of the smith chart (matching). Adding a series capacitance $C_1$ to our setup moves the point *DP1* along the circle counterclockwise till we reach the point *TP2*. From this point we reach the center by adding the parallel capacitance $C_2$. The resulting circuit is depicted in figure 5.5.

## 5.2 Tag IC matching

Matching the tag IC impedance to a 50 Ω load is treated analogous to the tag impedance matching. Using the table 4.1 from section 4 we can calculate the characteristic impedance for the different rectifier realizations. Bear in mind that the underlying model assumes the use of a parallel RC circuit. With an additional work step, we can calculate the values for the

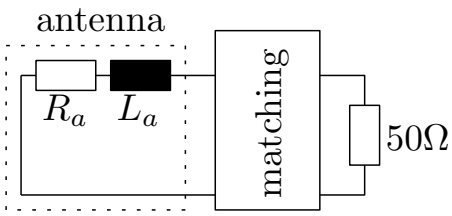


(a) Antenna impedance that is matched to a 50 Ω load

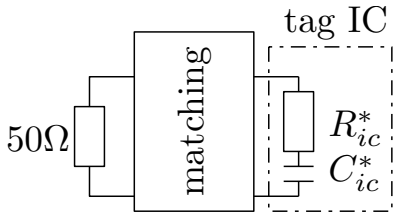


(b) Tag IC input port matched to a 50 Ω load

Figure 5.3: Matching the tag antenna and the tag impedance to 50 Ω

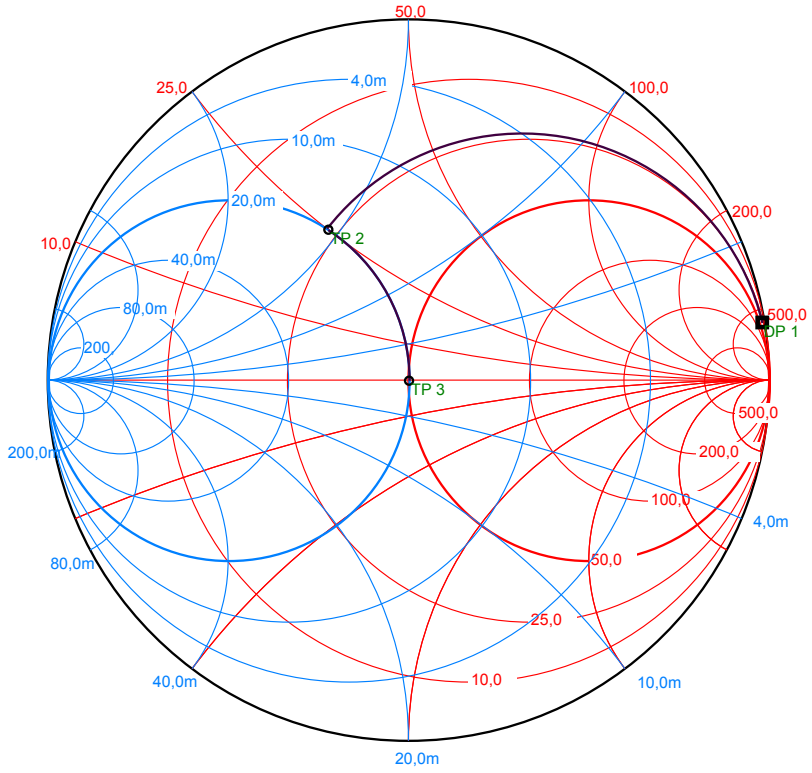


Figure 5.4: Smith chart visualizing the matching of the tag antenna

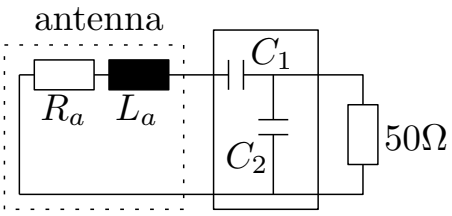


Figure 5.5: Antenna impedance that is matched to a 50 Ω load, $C_1$ =313 pF and $C_2$ =4 pF

equivalent RC series circuit. The circuit elements labeled with a star denote series topology whereas the missing star denotes values for parallel RC circuit.
The shut-series transform is used to convert the parallel circuit to a series circuit and vice versa. This is important since the values for the different rectifier realizations assume a parallel RC circuit. With the use of the equation which was derived in appendix A.3 we can calculate the values of the series circuit via equation 5.1c and 5.2a. Table 5.1 gives an overview of the calculated shunt resistor for the given rectifier realizations. Carefully inspecting equation 5.2a we notice that the influence of quality factor Q can be neglected. This is possible due to the high magnitude of the numerical value of Q. The reciprocal value

of the squared quality factor is close to zero.

$$R_{ic}^{*} = \frac{R_{ic}}{Q^2+1} = \frac{R_{ic}}{\left(\frac{R_{ic}^{*}}{X_{ic}}\right)^2 + 1)} \tag{5.1a}$$

$$= 16332.32 \cdot \frac{1}{\left(\frac{16332.32}{\frac{1}{2\cdot\pi\cdot 866\cdot 10^{6}\cdot 300\cdot 10^{-15}}}\right)^2 + 1} \tag{5.1b}$$

$$= 22.95\,\Omega \tag{5.1c}$$

$$X_{ic}^{*} = \frac{X_{ic}}{(1+Q^{-2})} \approx X_{ic} \rightarrow C_{ic} = C_{ic}^{*} \tag{5.2a}$$

| type | $R_{ic}$ | $R_{ic}^{*}$ |
|---|---|---|
| CTS | $37000\,\Omega$ | $10.14\,\Omega$ |
| UHF1 | $9400\,\Omega$ | $39.76\,\Omega$ |
| UHF2 | $3000\,\Omega$ | $120.09\,\Omega$ |
| UHF3 | $25000\,\Omega$ | $15.00\,\Omega$ |

Table 5.1: Shunt-series transform for different rectifier realizations

The calculation of matching circuit is performed for rectifiers CTS and UHF2. As in the example from before, the smith chart is used to design the matching network. Figure 5.6 display the smith chart that is used to match the UHF2 realization. As before the data point *DP1* denotes the impedance of the rectifier. The data point is located in the lower half of the smith chart due to the capacitive characteristic of the impedance. With the help of a parallel inductivity $L_1$ we reach the point *TP2* in the upper half of the smith chart. From this point a series impedance $C_3$ is used to reach $TP_3$. Figure 5.3a shows a picture of the obtained matching circuit.
In theory, additional circuitry between the tag antenna and the tag IC is considered as a reasonable approach. The increased power that is incident at the tag IC is supported by theory and simulations. In our case we notice that the initial matching between antenna and tag IC is close the optimum. We assume that the different rectifier realization just differ in their resistive components. The main aim of the matching network is to compensate the imaginary part of the impedance that represents the load.
Practical realization of an RFID tag try to avoid the use of a matching network. The increased effort that is needed to fabricate an RFID tag makes this approach less attractive. For that reason design methodologies favor implementations that require as little off-chip components as possible.

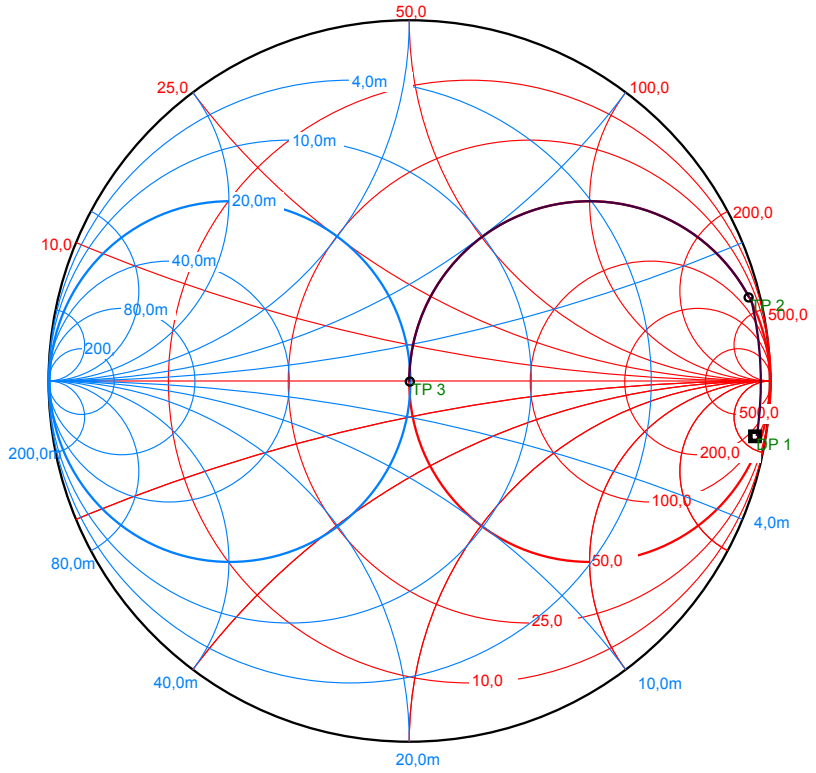


Figure 5.6: Smith chart visualizing the matching of the UHF2 rectifier

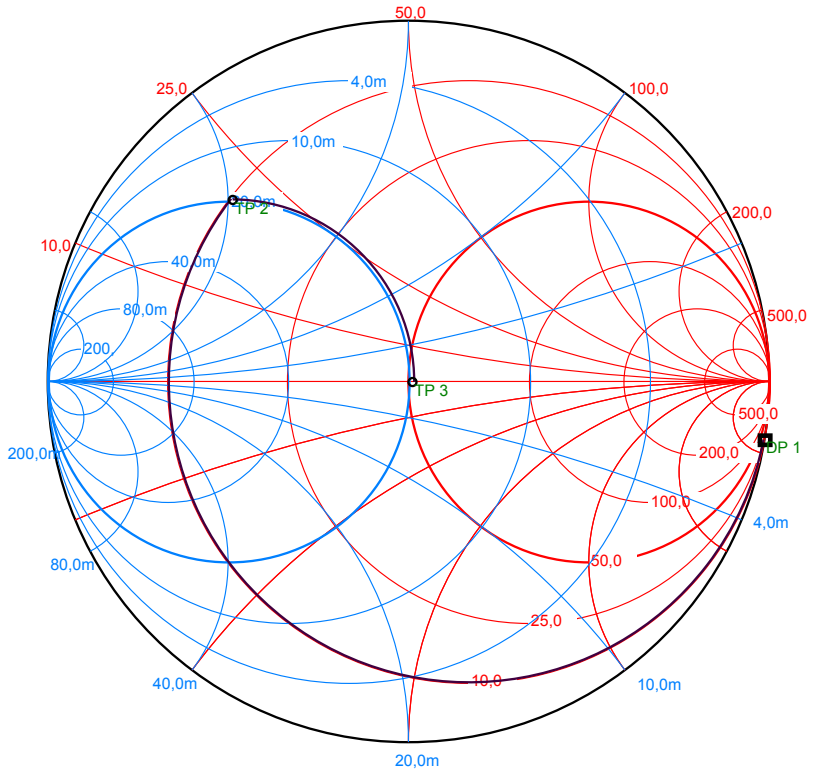


Figure 5.7: Smith chart visualizing the matching of the CTS rectifier

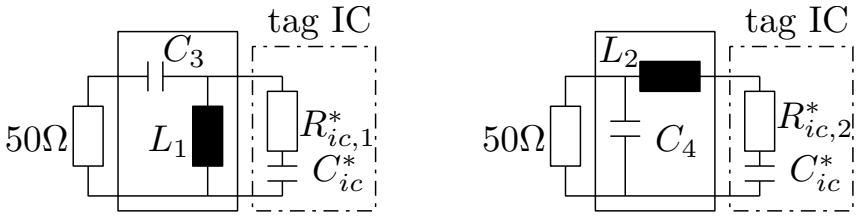


(a) Antenna impedance matched to 50 Ω with $C_3$ =459 fF and $L_1$ =45.6 nH

(b) Tag IC input port matched to 50 Ω with $C_4$ =7.2 pF and $L_2$ =116.3 nH

Figure 5.8: Matching the tag antenna and the tag IC to 50 Ω with matching circuit realization

# 6 Constructive Superposition

The previous chapter threated with the optimization of the signal transmission channel between sender and receiver. The main area of research was the matching between the tag antenna and the receiver IC. This approach is purely passive requiring no additional power source at the receiver. The strategy aims at increasing the power, which is delivered to the tag to the theoretical maximum. The signal power that is backscattered towards the reader is bound by power level that was originally received by the tag. Figure 6.1a shows a visual representation of the passive RFID communication scenario. In order to interpret the following figures properly keep in mind, that the reader is assumed to be placed left whereas the tag is found on the right. The arrow heads indicate the direction of the power flow. Whereas the width of the arrow is representative for the magnitude of the power level that is emitted. The picture in 6.1b depicts an application scenario that uses a tag that is equipped with an additional power source. In this case the power source at the tag is realized in form of a battery. In addition to the power received by the reader the power level of the backscattered signal is increased with help of the battery. This approach requires our setup to accurately synchronize to the carrier signal that is send out by the reader. Notice that this strategy requires the presence of a constant wave signal from the reader. There is another approach that is able to compensate for the fact which is discussed in section 7.

## 6.1 Varying the reflection coefficient

Thinking back to section 2.5.1 we can recall the principle of a wireless backscatter radio. Keep in mind that the power which is dissipated at the antenna resistor $R_a$ is emitted via the air interface. Increasing the current through resistor $R_a$ entails a higher amplitude of the backscattered signal. This fundamental principal is applied by an RFID tag to talk to the reader. A practical implementation uses a switch in form of a transistor which is

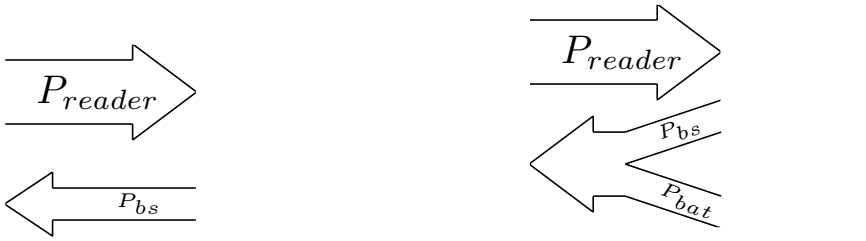


(a) detailed circuit diagram of the tag

(b) detailed receiving circuit with matching block

Figure 6.1: Receiving circuit with and without matching

parallel to the tag impedance (see figure 6.2). Careful readers surely noted that a variation in the antenna load implies a change of the reflection coefficient $S_{11}$. Assuming a modulation index of 100% and a data sequence consisting of alternating symbols allows us to sketch the evolution of the reflection coefficient and the terminal voltage $U_t$ over time (see figure 6.3). Figure 6.3a visualizes the change of reflection $S_{11}$ as a function of time. We can distinguish between two different states: With the switch in open position we realize that the value of $S_{11}$ is in the vicinity of zero (state labeled *matched*). Closing the switch causes a mismatch which can be perceived as an increase in the reflection coefficient (state labeled *short circuit*). The difference between those two states is denoted by $\Delta$. In literature this term is often denote as $\Delta rcs$. The letters *rcs* stand for *"radar cross section"* which is the difference of the effective area of the antenna in both modulated and non modulated states. Assuming a noisy communication channel the reader is barely able to properly receive the response from the tag. In this case we have to make sure to achieve a $\Delta rcs$ that enables the reader to differentiate between the two modulation states. Figure 6.3b plots the time-dependent course of the terminal voltage $U_t$. Analogously to the plot of the reflection coefficient in 6.3a, we notice two different states. If the antenna impedance is matching to the tag IC port the terminal voltage equals half of thhe voltage source $U_s$. Once the switch is closed we notice that the voltage across the antenna terminals is zero. Short circuiting the load increases the current through the receiving circuit, increasing the backscattered wave. Shorting the antenna terminals has a side effect on the power supply of passive RFID tags. As mentioned in section 2, passive tags harvest the energy from the surrounding electro-magnetic field. With a modulation index of 100% we effectively cut off the power supply to the tag. This is why the RFID standard specifies that the modulation coefficient to be less than 100% [6].

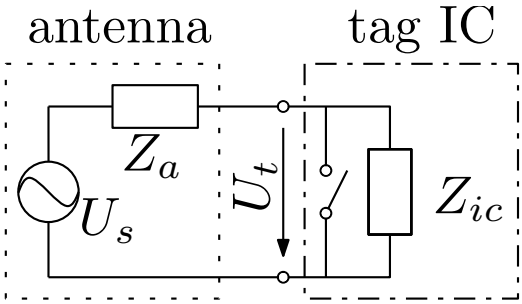


Figure 6.2: Receiving circuit with switch used for modulation

In order to increase the power of the backscattered signal, we have to find a possibility to increase the power dissipated at the impedance $Z_a$. Speaking more precisely, the backscattered power depends on the power dissipated at the ohmic part of $Z_a$. Under the assumption that we are facing a semi-passive transponder and we can utilize its battery to increase the magnitude of the tag's reply.

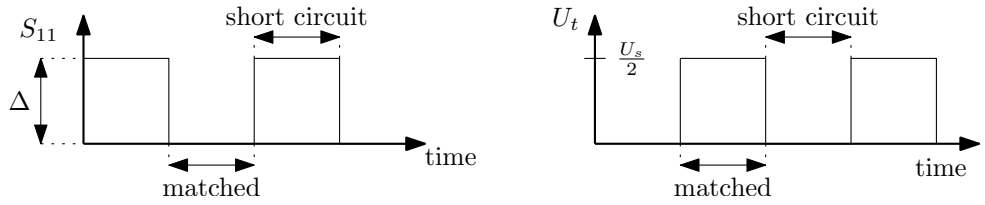


(a) $S_{11}$ variation over time (b) Terminal voltage $U_t$ over time

Figure 6.3: Reflection coefficient $S_{11}$ and terminal voltage as a function of time

## 6.2 Receiving circuit for active backscattering

As a first starting point we assume that the tag listens to the data which is sent from the reader. It this case the circuit ports 1 and 3 are shorted which represents the matched state as seen before. Instead of shorting the antenna terminals during modulation, we bridge ports 1 and 2. Note that there is either a connection between 1 and 3 or 1 and 3. Shorting ports 1 with 2 and 3 at the same time is not intended. The circuit diagram in figure 6.4 visually underlines this paragraph. As before we can plot the terminal voltage $U_t$ as a function of time.

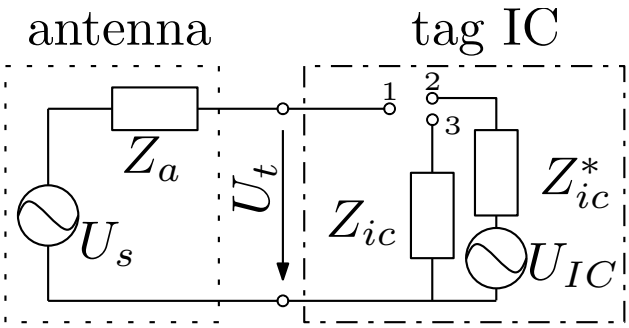


Figure 6.4: Receiving circuit supporting active backscattering

For the next considerations we assume that the we are in active modulation mode (there is a connection between the circuit ports 1 and 2). Before going into detail about the exact calculation of $U_t$ let's spend a moment to think about factors that influence the terminal voltage. Assuming that the impedance $Z^*_{ic}$ is zero it is obvious that the resulting terminal voltage is equivalent to the voltage $U_{ic}$. The lower the impedance which is in series to the voltage source, the stronger its influence on the terminal voltage. Furthermore we notice, that the resulting terminal voltage $U_t$ is directly proportional to the voltage $U_s$ and $U_{IC}$. With the help of the superposition principle we can calculate contributions of each of them to $U_t$. While calculating the voltage $U'_t$ we assume that the voltage source $U_{ic}$ is shorted. The same holds true for the calculation of $U''_t$ whereas the voltage source $U_s$ is short circuited (see equation 6.1 and 6.2).

$$U'_t = U_s \cdot \frac{Z_{ic}}{Z_{ic} + Z^*_{ic}} \tag{6.1}$$

$$U_t'' = U_{ic} \cdot \frac{Z_{ic}^*}{Z_{ic} + Z_{ic}^*} \tag{6.2}$$

Figure 6.5 outlines the resulting terminal voltage $U_t$ due to $U_s$ and $U_{ic}$. Voltages $U_t'$ and $U_t''$ are the individual terminal voltages that are caused by $U_s$ and $U_{ic}$.

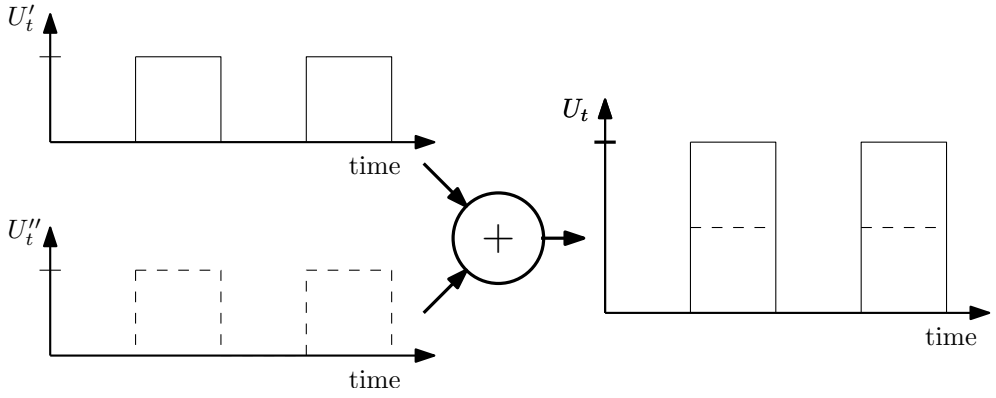


Figure 6.5: Terminal voltage being a superposition of $U_s$ and $U_{ic}$

The plots in figure 6.5 use a simplified illustration of the voltages. On a closer inspection of the circuit diagram in figure 6.4 we notice the sinusoidal voltage sources. Despite the amplitude of the voltage source we realize that there is another factor that influences the terminal voltage. We already discussed the influence of the impedance and the amplitude of the voltage source. Another parameter that has an impact on the terminal voltage is their phase relation of the two voltage sources. Figure 6.6 outlines the influence of the phase difference $\varphi$. In plot 6.6a we notice the effect of constructive interference. In this case $U_t'$ and $U_t''$ are in phase and yielding a terminal voltage which is the sum of the individual amplitudes. A phase difference of $\pi$ implies that we are faced destructive interference (see figure 6.6b). As soon as the voltage $U_t'$ reaches its maximum, $U_t''$ has a minimum and vice versa.
The following simulation is focused on varying the phase difference between $U_t'$ and $U_t''$. Figure 6.6 was concerned with two special cases of $\varphi$. With a linear variation of the phase difference we try to deduce its impact on the resulting signal power. To start our investigations we first have to develop a strategy that lets us calculate the signal power. As a first starting point we compute the signal power for an in-phase sinusoidal signal which is depicted in figure 6.6a. The statistical measure called quadratic mean or root mean square (RMS) is used to express the power of a signal. Equation 6.3 states how the calculation is performed of a continuous

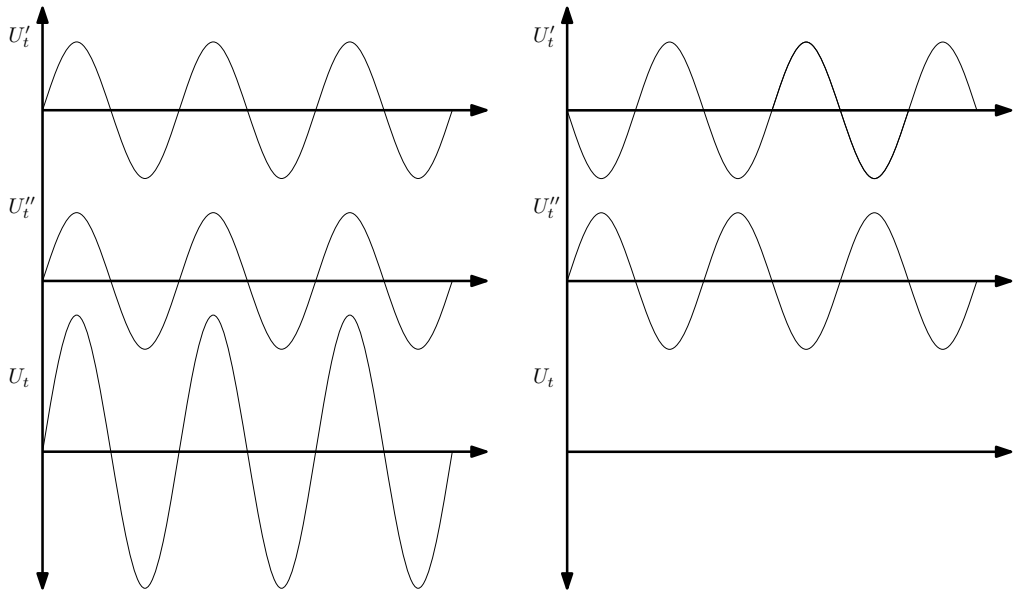


(a) Constructive interference for $\varphi = 0$ (b) Destructive interference for $\varphi = \pi$

Figure 6.6: Interference is a function of the phase difference between $U_t'$ and $U_t''$

signal that is defined in the interval $T_1$ to $T_2$ with the duration $T$.

$$P_{rms} = \sqrt{\frac{1}{T_2 - T_1} \int_{T_1}^{T_2} f(t)^2 dt} \overset{f(t)=a \cdot sin(t)}{=} \sqrt{\frac{1}{T-0} \int_0^T a^2 \cdot sin(t)^2 dt} \tag{6.3a}$$

$$\overset{sin(t)^2 = \frac{1-cos(2t)}{2}}{=} \sqrt{2 \cdot a^2 \cdot \frac{1}{2 \cdot \pi} \int_0^{\pi} \frac{1 - cos(2t)}{2} dt} \tag{6.3b}$$

$$= \sqrt{\frac{a^2}{\pi} \left[ \frac{1}{2} \cdot t \Big|_0^{\pi} - \frac{1}{2} \cdot \frac{sin(2t)}{2} \Big|_0^{\pi} \right]} = \sqrt{a^2 \cdot \frac{\pi}{2 \cdot \pi} - 0} \tag{6.3c}$$

$$= \frac{a}{\sqrt{2}} \tag{6.3d}$$

Think back to the example in figure 6.6a: We assume that the voltages $U_t'$ and $U_t''$ both have amplitudes of 1 V each. Adding these voltages equals a terminal voltage of 2 V. We can use this parameter to calculate the resulting power $P_{rms}$ (see equation 6.4).

$$\frac{a}{\sqrt{2}} \overset{a=2}{=} \frac{2}{\sqrt{2}} = 1.414 \tag{6.4}$$

The following simulations were performed with the numerical computing environment MATLAB® [18] that operates on discrete data. In this case we have to rewrite equation 6.3 to be valid for discrete signal processing. First of all we have to define the structure of signal

vector $X$ which can be found in equation 6.5. Equation 6.6 requires the squaring of signal vector $X$ which is formally described by 6.7.

$$X = [x_1, x_2 \cdots x_N] \tag{6.5}$$

$$p_{rms} = \sqrt{\frac{1}{N}\sum_{i=0}^{N-1} x_i^2} = \sqrt{\frac{1}{N} \cdot X \cdot X^T} = \sqrt{\frac{1}{N}\overline{X^2}} \tag{6.6}$$

$$X^2 = \left[x_1^2, x_2^2 \cdots x_N^2\right] \tag{6.7}$$

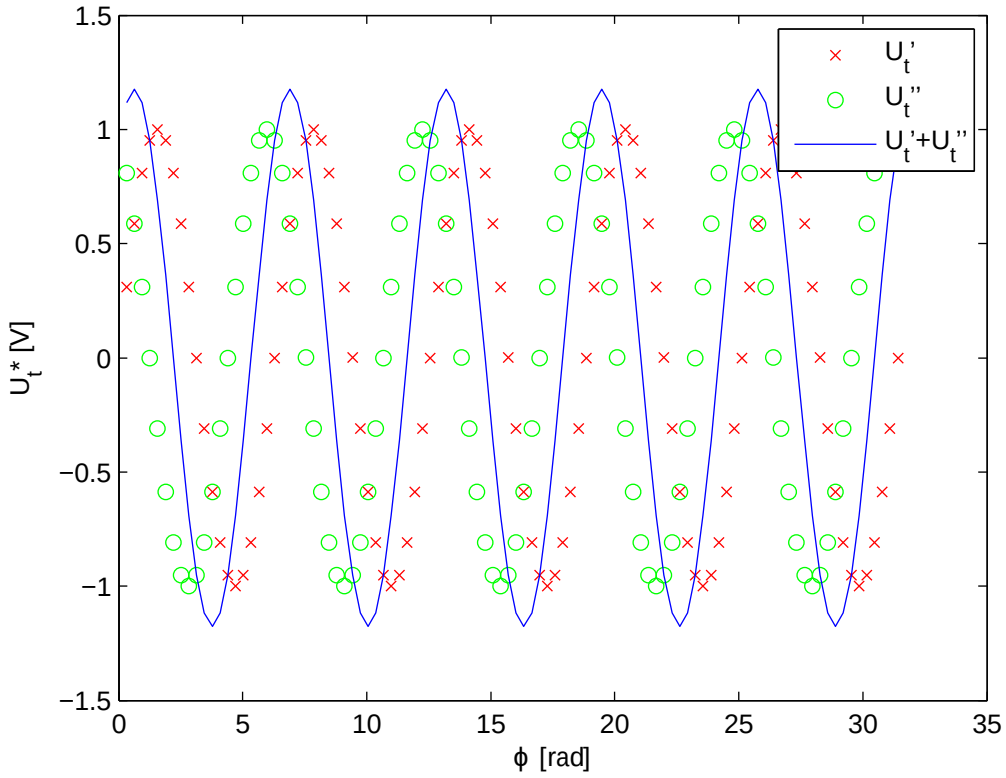


Figure 6.7: Signal curve of the terminal voltage for a phase difference $\frac{3\cdot\pi}{5}$ between $U_t'$ and $U_t''$

Once we have established a metric that helps us measuring the signal power we can start the simulation. We vary the phase difference between $U_s$ and $U_{ic}$ and observe the impact on the power of the resulting terminal voltage. The value range of $\varphi$ is defined from 0 to $2 \cdot \pi$. The simulation uses equidistant steps of $\frac{\pi}{5}$ which equals 10 simulation points within the range of 0 and $2 \cdot \pi$. The results of the afore mentioned simulation can be seen in figure 6.5. Inspecting 6.5 we notice two distinctive points. For the case of the two in-phase signals ($\varphi$=0) we notice that the resulting value from the simulation perfectly corresponding to the value which we initially had derived in 6.4. A phase difference of $\pi$ entails that the value for $p_{rms}$ is close to zero. This fact is underlined by the figure which can be found in 6.6b. Another thing that we

notice is the symmetry point that is located at $\varphi = \pi$. The reason for that is the symmetry of sinusoidal signal $U_t'$ and $U_t''$.

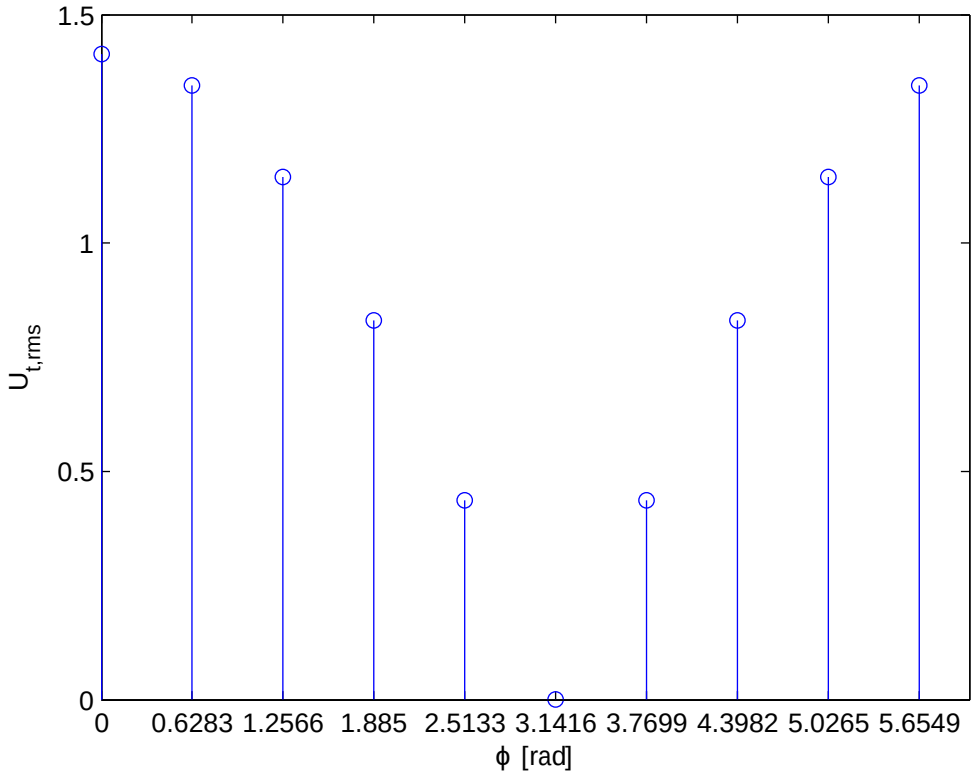


Figure 6.8: Resulting terminal voltage vs. phase difference between $U_t'$ and $U_t''$

# 7 Active transmitting architecture

This chapter introduces the system architecture for an RFID tag that implements active backscattering. We use the term active backscattering to denote that the reply sent to the reader is amplified at the transponder. As already mentioned before, we know that passive and semi-passive RFID transponders solely reflect the power sent out by the reader. Its open to debate whether or not the term active backscattering is still adequate, because the constant wave from the reader is not reflected at the tag. We notice that the backward-channel of our novel system is comparable to an active RFID system.
The newly proposed system design utilizes a tag with additional power source. Figure 7.1a pictures the passive scenario from the previous section. We see that the reflected wave is a portion of the power that was originally sent from the reader. Figure 7.1b depicts the scenario in which the active backscattering architecture is used. The power level $P_{bat}$ is caused by the power source of the transponder. In this case the power source is represented by a battery. From this follows the essential difference between the two approaches. Positive interference combines the signal received from the reader and a signal that is internally generated. The new approach favors the power source as a exclusive resource for the power of the reply that is sent to the reader.
The original form of a PLL serves as the basis for deriving the architecture of an active backscattering system. First of all we have to create a simulation environment, which can be used to test the validity of the newly derived model. As a first starting point we have to model a PLL in it's most basic form. Recalling the block diagram from 2.6 depicting the block diagram of an ordinary PLL.
In our case we restrict our investigations to analog PLLs. We use the numerical simulation environment MATLAB® to analyze the behavior of our setup. All simulations are performed in discrete-time. Two real-life examples are used to familiarize with the working principles of a PLL. Having understood the fundamental principle of a PLL, we can use it to develop a new architecture that is used for realizing an active backscattering system.


(a) State of the art passive scenario

(b) Semi-passive scenario using active backscattering

Figure 7.1: Passive/semi-passive communication scenario with different power levels

## 7.1 Practical example I

The PLL used by our simulation uses a multiplier as a phase/frequency detector. The loop filter is realized in form of a second-order filter. Figure 7.2 depicts the block diagram of the PLL. We can see the loop filter consisting of two signals path. The filter coefficient $b_0$ is located in the direct path of the loop filter. It is used to weight the phase difference of the current samples of the reference signal and the output signal *"fout"*. The impact of the phase difference from samples from the past are weighted by the factor $a_0$. As we have already heard in the fundamentals section, the behavior of the VCO is described by two parameters. The characteristic curve is defined by the center frequency $f_c$ and the slope $K$. Table 7.1 states the parameters used in the simulation.

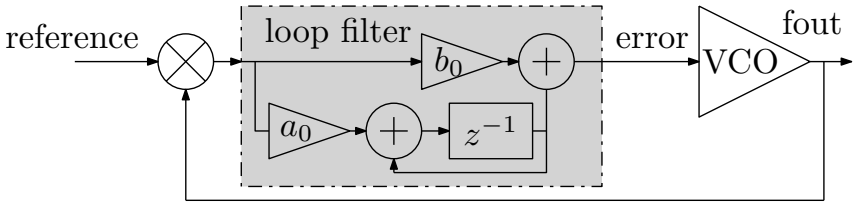


Figure 7.2: Block diagram of the PLL architecture that is used in the simulation

| | |
|---|---|
| $a_0$ | 0.200 |
| $b_0$ | 0.010 |
| $K$ | 0.001 |
| $f_{ref}$ | 866 MHz |
| $f_{sample}$ | 2 GHz |

Table 7.1: PLL simulation parameters

The first simulation scenario assumes, that there is a frequency deviation between the reference signal and the sinusoidal signal generated via the VCO. The loop filter blocks unwanted frequency components that are a result of the mixer-based phase/frequency detector. The error signal is proportional to the phase/frequency difference between the output signal and the reference signal driving the VCO. The feedback signal is the last piece that completes the structure of a control system.
From the simulation we can get an insight on the locking behavior of the PLL. We can see the influence of the different parameters and recognize the different states of a PLL. Figure 7.3 depicts the signal curve of the error function over time. In the plot we can find two versions of the error signal. There is the original error signal directly taken from the simulation. The other signal trace is the error signal smoothed with a moving average filter with 20 taps. The simulation was carried out with a frequency difference between the reference signal and the output signal of 15 MHz. During the time span from 0 ns to approximately 200 ns we notice a steep increase in the error function. After we pass the point of 200 ns we notice a stagnation of the error signal. Inspecting the region of convergence, we notice that the error signal reaches its steady state around the value of 6.5. In order to tell whether the obtained

value is correct we have to look into the details of the locked state of a PLL.

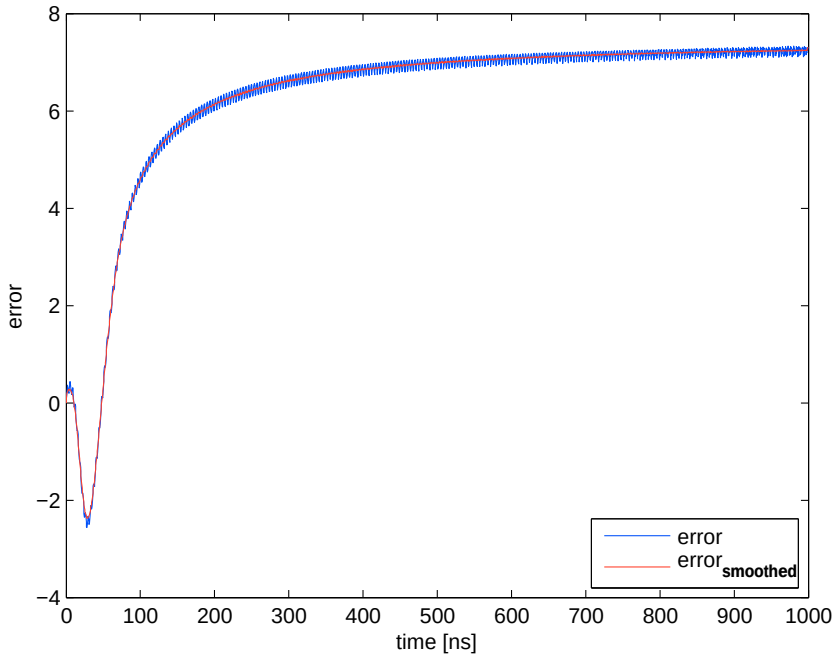


Figure 7.3: Evolution of the error signal for a frequency difference $\Delta f = 15\,MHz$

Under the assumption that the PLL is locked, we know that the phase of reference and output signal is equal. Since our simulation uses discrete time we have to declare a sampling frequency $f_{sample}$. The sampling frequency is a measure for the number of evaluation points per time. Equation 7.1a and 7.1b state how the reference signal and the output signal are calculated.

$$f_{out} = cos\left(2 \cdot \pi \left[\frac{f_{ref}}{f_{sample}} + K \cdot error\right]\right) \tag{7.1a}$$

$$reference = sin\left(2 \cdot \pi \left[\frac{f_{ref} + \Delta f}{f_{sample}} + \Delta\varphi\right]\right) \tag{7.1b}$$

When the PLL is locked, we know that both signals are in phase ($arg(f_{out}) \stackrel{!}{=} arg(reference)$). Using this fact, equation 7.2 compares the arguments of the two signals.

$$\begin{aligned} &= 2 \cdot \pi \left[\frac{f_{ref}}{f_{sample}} + K \cdot error\right] = 2 \cdot \pi \left[\frac{f_{ref} + \Delta f}{f_{sample}} + \Delta\varphi\right] \\ \stackrel{\Delta\varphi=0}{\rightarrow} &\frac{f_{ref}}{f_{sample}} + K \cdot error = \frac{f_{ref} + \Delta f}{f_{sample}} \end{aligned} \tag{7.2}$$

Taking the steady state error from figure 7.3 and placing it in equation 7.2 we can show that the PLL simulation yields realistic results. As mentioned before we assume that the error in

steady state is around 6.5. Equation 7.2 uses the values as in table 7.1 and the steady state error.

$$\frac{f_{ref}}{f_{sample}} + K \cdot error = \frac{f_{ref} + \Delta f}{f_{sample}} \tag{7.3a}$$

$$= \frac{866e6}{2e9} + 0.001 \cdot 6.7 = \frac{866e6 + 15e6}{2e9} \tag{7.3b}$$

$$= 0.4395 \approx 0.4405 \tag{7.3c}$$

The small variance between the values in equation 7.3 can be justified by the fact that the value for the steady state error was read from the simulation. We can conclude that our simulation delivers realistic steady state values for the error signal that are at least in the vicinity of the true value.

## 7.2 Practical example II

Figure 7.4 shows the results of another practical example, which builds on the simulation from before. In this case the frequency difference $\Delta f$ is increased up to 80 MHz, observing the impact on the error signal. It can be seen in figure 7.4 that the increased frequency difference causes an error signal which is significantly higher that in the previous case. Since the parametrization of the system stays the same, we are using the same time interval to adjust the output signal *"fout"* to the reference input signal. After 500 ns we see the error slowly converging. It is not obvious to see the exact value the error signal converges to. Assuming that we approach a value between 35 and 40, we choose 37.5.
Putting the steady state value of 37.5 and the altered frequency difference $\Delta f$ into equation 7.2, we can calculate the individual arguments of the reference signal and the output signal as in the previous scenario.

$$\frac{f_{ref}}{f_{sample}} + K \cdot error = \frac{f_{ref} + \Delta f}{f_{sample}} \tag{7.4a}$$

$$= \frac{866e6}{2e9} + 0.001 \cdot 37.5 = \frac{866e6 + 80e6}{2e9} \tag{7.4b}$$

$$= 0.4705 \approx 0.473 \tag{7.4c}$$

From the simulation we notice that a locked PLL is marked by a converging error function. Automatically detecting if a PLL is locked requires it to develop a criterion that predicates this state. Section 7.3 is devoted to solve this challenge.

## 7.3 Automatic lock detection and PLL freezing

This section assumes that the parameters of the PLL are chosen to fulfill the stability criterion. For the course of this section we assume that the conditions met to achieve a PLL lock. In order to automatically detect if a PLL is locked, we have to develop a suitable algorithm.

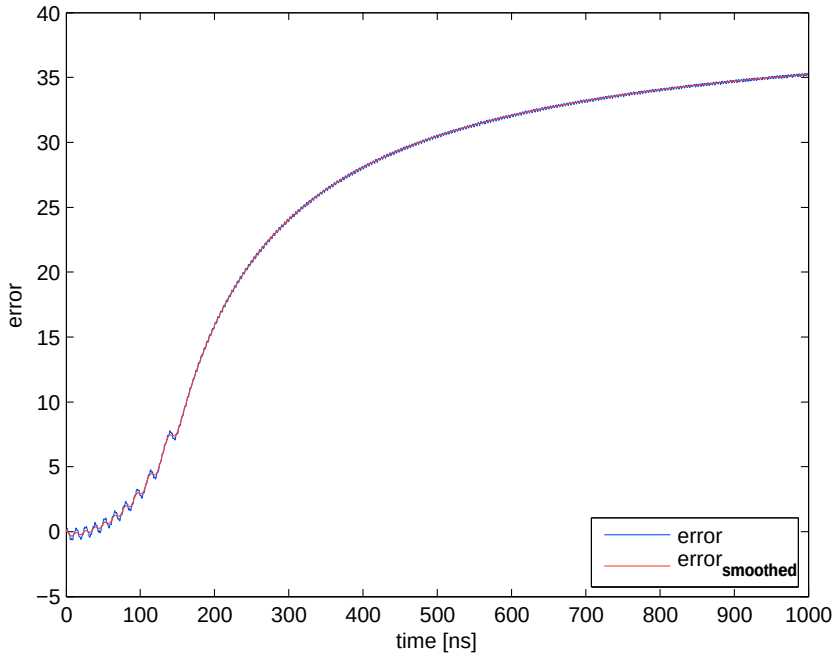


Figure 7.4: Evolution of the error signal for a frequency difference of 80 MHz

In section 7.1 we have already seen the evolution of the error as a function of time. During the initial phase we saw that there is quite a large fluctuation in the magnitude of the error function. After some time we noticed that the error function approached a fixed value. We notice that there is a certain point in time where the fluctuation of the error function was below a certain threshold level. After this point we have attained synchronization between the input and the output signal. Mathematically speaking, this time range is denoted by the fact that the gradient of the signal is close to zero. Differentiating the error signal, we can detect the point that marks the start of steady state.
Figure 7.5 shows two exemplary signals demonstrating the effect of the gradient operator. The left figure 7.5a plots the course of a triangular signal. The triangular signal can be described with to linear equations, whereas the first part of the signal has positive slope and the second part a negative one (signal with dots). If we apply the differentiation on the triangular wave, we get a rectangular waveform (signal denoted with stars). This totally agrees with the fact that the triangular wave can be described by two linear equations.
The signal on the right in plot 7.5b shows a polynomial of $2^{nd}$ degree. As in the plot before we use dots and stars to denote the two different signals. Inspecting the course of the polynomial, which is evaluated between $-1$ and 1, we can see that it flattens at a value close to zero. This is underpinned by the fact, that the derivative of $x^2$ is $2 \cdot x$ which is a linear function.
We are not concerned about the sign of derivative of the error function. The only criterion used during our decision making is the magnitude of the error. In order to perform the thresholding we have to define the value of $\epsilon$. We say that the PLL is locked if we happen to see the first value of the error function that is smaller than the given $\epsilon$. The block diagram

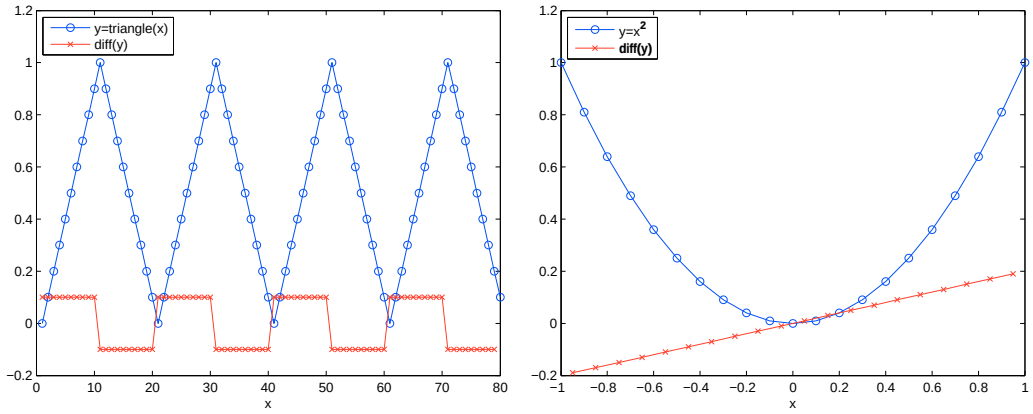


(a) Triangular wave and the corresponding slope

(b) First order polynomial and it's derivative

Figure 7.5: Numerical differentiation shown with the help of two exemplary signals

in 7.6 visualizes the signal processing block that implements the lock detection. The block labeled *"moving avg."* is a moving average filter that smoothens the signal before the gradient is computed. This step adds more robustness to the lock detection mechanism. Far on the right we find a block called *"freeze VCO"*, which outputs the VCO voltage in case of a missing reference signal.

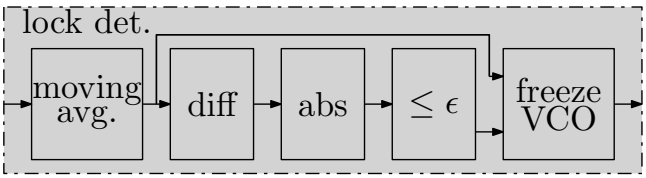


Figure 7.6: Signal processing blocks implementing a PLL lock detection

Figure 7.7 uses the signal processing block as depicted in figure 7.6. This is applied to the error function that was already shown in figure 7.3. The dashed line denotes the point that is found via the lock detection. We use this point and go back to the plot of the error function from before. The figure in 7.8 depicts the course of the error function. In addition to that we can see the point that marks the PLL lock. Starting from this point to the end of the simulation we calculate the average mean of the error function. The black squared box in figure 7.8 denotes the time interval of the error function that is used to calculate the VCO offset. This value appears at the output of the *freeze VCO* block from figure 7.6.

## 7.4 Putting it all together

What is left to do is the combination of the earlier discussed subsystems. The basic system consists of a PLL in its most essential form. This system is extended with the lock detection discussed in previous section. A signal processing block that increases the signal power of the

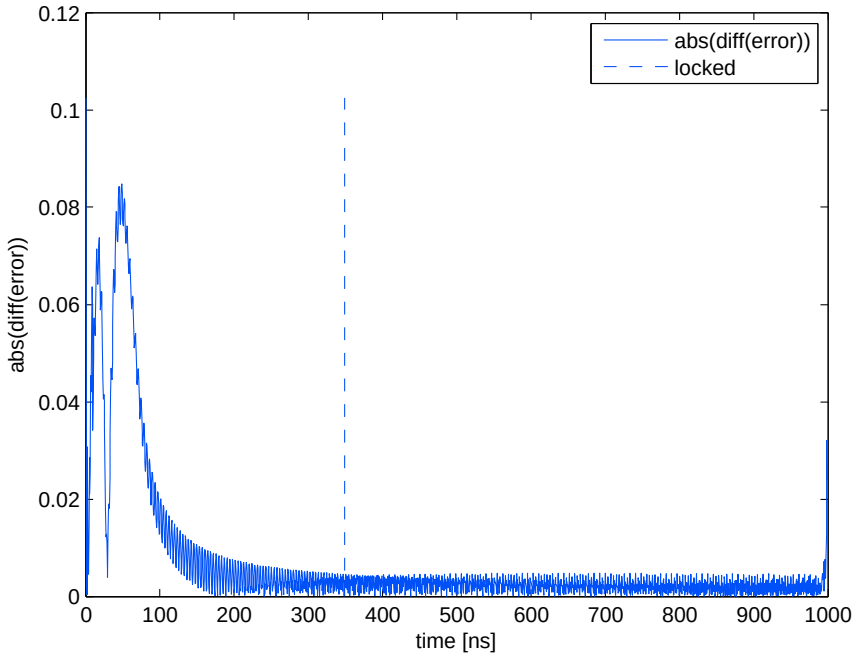


Figure 7.7: Magnitude of the gradient of the error function for $\epsilon = 0.0002$

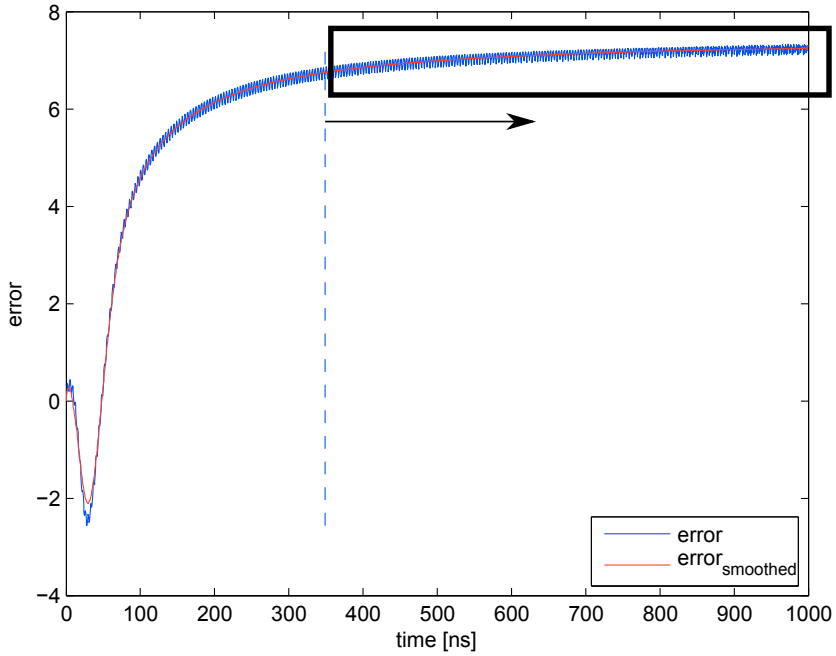


Figure 7.8: Error signal for $\Delta f = 15\,MHz$ with the dotted line indicating a PLL lock

backscattered signal. Analog circuitry is used to seperate the received signal and the signal to be transmitted. Figure 7.9 depicts the resulting active backscattering system. In order to understand the overall system of the active transmitting architecture we traverse the picture from left to right, explaining each individual block, their properties and the interconnection with other parts pf the system.

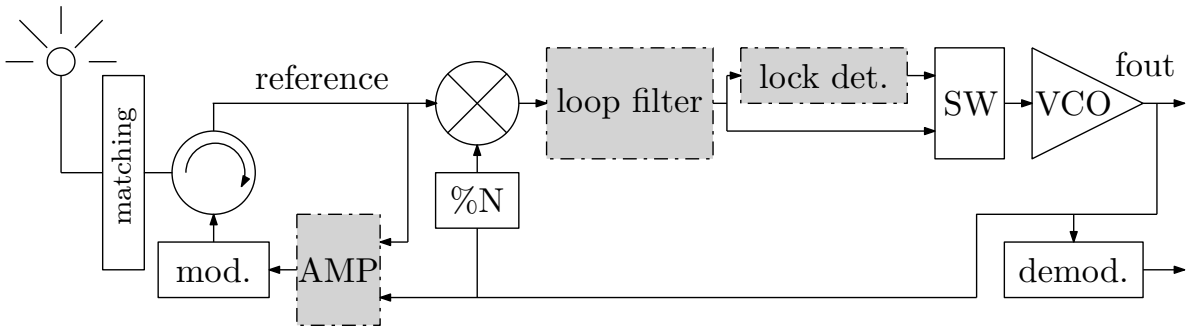


Figure 7.9: PLL architecture implementing active backscattering

The vertical block labeled *"matching"* ensures impedance matching between the tag antenna and the transponder IC. As before mentioned we need this mechanism that allows us to separate the signal received via the antenna and the signal we were going to transmit. This is accomplished by using a circulator. The wire labeled *"reference"* is the input to the PLL control loop. The new thing here is the gray shadowed block implementing the lock detection. A PLL that tries to track the frequency of the reference signal drives the VCO with a filtered version of the phase/frequency comparator. Once the PLL is locked, the lock detection block derives an averaged steady state value of the error signal that is used as an input to the VCO. The SW block, which is an abbreviation for *"switch"*, is used to control which input signal appears at the output of this block. There is a gray block lettered with AMP. The internal decomposition of this block can be found in figure 7.10. It is mainly used to choose the method of how the backscattered signal is generated.
In general there are two approaches: One of them uses the same principle already described in section 6. We use the upper signal path of the AMP block and add the reference signal to the output signal *"fout"*, considering their phase relationship. The other approach is used if no reference signal is available. In that case the backscattered signal is a purely synthesized version of the reference signal. This signal is amplified by the gain G and then sent to the reader.

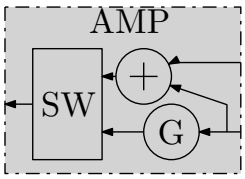


Figure 7.10: Internal realization of the amplifier block

The picture in 7.11 plots the time domain simulation of the active backscattering system. On closer inspection we notice that the simulation can be divided into three time ranges. During the first period the PLL adjusts it's frequency/phase to track the input signal. Once reference signal and output signal are synchronized, we notice flattening in the course of the error function. The lock detection recognizes the steady state. By calculating the mean of the error signal during this time span, it allows us the calculate a steady state error which is used as an input to the VCO. During the next stage we open the control loop formed by the PLL. In this case the resulting output frequency is determined via the steady state value just computed. Starting from the locking point we notice that the magnitude of the error signal increases linearly. This can be explained with the tracking behavior of the PLL experiencing a small control error. Due to the fact that the control loop was opened, we are not able to compensate for the current error, which means that the phase difference between input signal and output signal gets bigger and bigger.

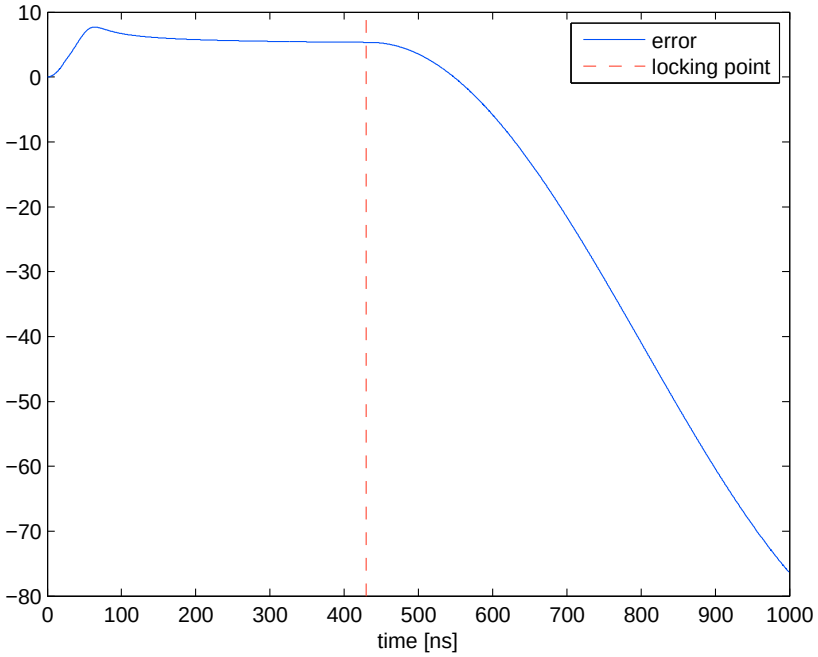


Figure 7.11: Timing curve of the error signal of the overall active backscattering system

# 8 Conclusion

The objective of this thesis is the analysis of current UHF RFID communication systems in respect to the factors limiting the read range. Three approaches were introduced that can be used to increase the read distance of the communication.

## 8.1 Summary and Results

As a first starting point the link budget of a state of the art RFID communication scenario was analyzed. An essential part of this analysis was carried out with the help of the generic path loss formula. Assuming that the propagation is free space we can use the Friis equation to calculate the attenuation for a given distance. Reordering of the Friis equation allows us the calculate the maximum possible distance if we are given a transmission power of the sender and the receiving sensitivity of the opposing party. The transformation of the Friis equation to logarithmic domain makes it possible to draw a visual representation of the link budget. The calculations were made for both passive and semi-passive RFID tags. Getting to know the impact of the individual parameters allows us to choose the proper strategy to increase to read range.

One approach to increase the read distance is focused on the matching between tag antenna and tag IC. There is a special form of the Friis equation which calculates the power delivered to the tag. By introducing an additional matching circuit between tag antenna and tag IC we can increase the available power to the theoretical limit. Using the *"Smith chart"* we can graphically design the matching circuit. This approach is considered to by straightforward and effective but the available power at the tag is still bounded the theoretical limits.

Another approach to overcome the theoretical restrictions is to increase the signal power with the use of positive interference. The carrier sent out by the reader is received by the tag. A semi-passive tag is equipped with a battery that allows us to generate another sinusoidal wave. If both waves are added in respect to their phasing, we end up with another sine wave increased in its amplitude. For succeeding with this approach it is crucial to achieve the proper phase between the two sine waves.

Last but not least the active transmitting architecture, which relies on the working principle of a phase locked loop (PLL). This approach is far more complex than the previously mentioned ones. Nevertheless it is also the most powerful one. Once the carrier is received, a control loop tries to run after the frequency of the given carrier signal. As soon as the input and the output signal have the same frequency, we consider the PLL to be locked. A dedicated signal processing block is used to detect this case and freeze the frequency of the output signal.

This means that we are able to talk back to the reader, even if the carrier signal of the reader is currently not available.

## 8.2 Future work

This thesis focused on principles that can be used to increase the reading distance of RFID communication, assuming the use of a new transponder design. The suggested approach requires new features that have to be implemented by the tag. Due to that reason the design gets more complicated and results into higher manufacturing costs of each tag. We realize that we are still able to use an off-the-shelf RFID reader without having to develop a new one.

Another idea to implement active backscattering involves the development of a new RFID tag architecture and an RFID reader as well. Instead of changing the design of the RFID tag on its own, this approach tries to balance the extra complexity between reader and tag. A drawback of this approach is the fact that the design might not agree with the RFID standard.

Once active backscattering is successfully implemented, we are faced with new challenges in applications that involve a large amount of tags. Indoor RFID applications suffer from multipath propagation. This means that the backscattered signal from the tag to the reader is sent along different propagations paths that entail different signal propagation delays. In order to be able to distinguish between individual tags that are in the vicinity of the reader and those that are further away, requires the implementation of a localization mechanism. The PhD thesis in [1] recommends a variate of principles that can be used to implement tag localization.

# Nomenclature

ETSI European Telecommunications Standards Institute

FSPL Free space loss

IC Integrated circuit

PLL Phase locked loop

RADAR Radio Detection and Ranging

RCS Radar cross-section

RFID Radio Frequency Identification

tag Transponder

tag IC Transponder integrated circuit

VCO Voltage controlled oscillator

# Bibliography


[1] *Tag localization in passive uhf rfid*, phdphd thesis, May 2011, Please contact daniel.arnitz@ieee.org for the full document. .

[2] Constantine A. Balanis, *Antenna theory: Analysis and design*, Wiley-Interscience, 2005.

[3] D.K. Banerjee and National Semiconductor Corporation, *Pll performance, simulation, and design*, Dean Banerjee Publications, 2001.

[4] Daniel M. Dobkin, *The rf in rfid: Passive uhf rfid in practice*, Newnes, Newton, MA, USA, 2007.

[5] K.L. Du and N.S. Swamy, *Wireless communication systems: From rf subsystems to 4g enabling technologies*, Cambridge University Press, 2010.

[6] Klaus Finkenzeller, *Rfid handbook: Fundamentals and applications in contactless smart cards and identification*, 2 ed., John Wiley & Sons, Inc., New York, NY, USA, 2003.

[7] IEEE P802.15 Working Group for Wirless Personal Area Networks (WPANs), *Channel model for body area network (ban)*, IEEE P802.15 Wirless Personal Area Networks (2009).

[8] Dellsperger Fritz, *Homepage that hosts the* `smith.exe` *software*, October 2013, http://www.fritz.dellsperger.net/.

[9] J. Grosinger and M. Fischer, *Evaluating on-body rfid systems at 900 mhz and 2.45 ghz*, RFID Technology (EURASIP RFID), 2012 Fourth International EURASIP Workshop on, 2012, pp. 52–58.

[10] Jasmin Grosinger, *Feasibility of backscatter rfid systems on the human body*, EURASIP Journal on Embedded Systems **2013** (2013), no. 1, 2.

[11] ANSYS HFSS, *A industry standard for simulating 3-d full-wave electromagnetic fields*, October 2013, http://tinyurl.com/kdsdnkf.

[12] ETSI European Telecommunications Standards Institute, *Radio Frequency Identification Equipment operating in the band 865 Mhz to 868 MHz with power levels up to 2W; Part 1*, Final draft ETSI EN 302 208-1 (2006).

[13] Griffin J.D. and Durgin G.D., *Complete link budgets for backscatter-radio and rfid systems*, Antennas and Propagation Magazine, IEEE **51** (2009), no. 2, 11–25.

[14] R.J.M.A.S.K. John D Kraus, *Antennas and wave propagation: Fourth edition*, Tata McGraw Hill, 2006.

[15] U. Karthaus and M. Fischer, *Fully integrated passive uhf rfid transponder ic with 16.7-mu;w minimum rf input power*, Solid-State Circuits, IEEE Journal of **38** (2003), no. 10, 1602–1608.

[16] G. Marrocco, *The art of uhf rfid antenna design: impedance-matching and size-reduction techniques*, Antennas and Propagation Magazine, IEEE **50** (2008), no. 1, 66–79.

[17] ———, *The art of uhf rfid antenna design: impedance-matching and size-reduction techniques*, Antennas and Propagation Magazine, IEEE **50** (2008), no. 1, 66–79.

[18] MATLAB, *version 7.10.0 (r2010a)*, The MathWorks Inc., Natick, Massachusetts, 2010.

[19] Gebhart Michael, *Rfid systems*, University Lecture, 2013.

[20] Nikitin P.V. and Rao K.V.S and Lam S., *UHF RFID characterization: Overview and State-of-the-Art*, AMTA 2012 Symposium (2012).

[21] P. Pursula, M. Hirvonen, K. Jaakkola, and T. Varpula, *Antenna effective aperture measurement with backscattering modulation*, Antennas and Propagation, IEEE Transactions on **55** (2007), no. 10, 2836–2843.

[22] Nikitin P.V. and Rao K.V.S., *Performance limitations of passive UHF RFID systems*, Antennas and Propagation Society International Symposium 2006, IEEE, 2006, pp. 1011–1014.

[23] ———, *Theory and measurement of backscattering from RFID tags*, Antennas and Propagation Magazine, IEEE **48** (2006), no. 6, 212–218.

[24] Theodore Rappaport, *Wireless communications: Principles and practice*, 2nd ed., Prentice Hall PTR, Upper Saddle River, NJ, USA, 2001.

[25] Gabriel S, Lau RW, and Gabriel C, *The dielectric properties of biological tissues: Iii. parametric models for the dielectrical spectrum of tissues*, Phisics Deparment, King's College, Strand, London, UK **2013** (2013).

[26] Agilent Technologies, *Advanced design system (ads)*, October 2013, http://www.home.agilent.com.

# Appendix

## A.1 Log-normal distribution

Empirical experiments have shown, that the power distribution across a wireless link is best described by the log-normal distribution. The log-normal distribution is best described as a product of a large number of independent, identically-distributed variables. The difference to the normal distribution is the fact, that the normal distribution is based on the sum of a large number if independent, identically-distributed variables.
The effect of shading can be explained by the obstacles along the propagation path. Each individual influence is superimposed and manifests at the receiver side as a variation around the mean of the received power. Equation A.1 is the mathematical representation of the log-normal distribution.

$$N(x, \mu, \sigma) = \frac{1}{x \cdot \sigma\sqrt{2 \cdot \pi}} \cdot e^{-\frac{ln(x-\mu)^2}{2 \cdot \sigma^2}} \tag{A.1}$$

Where $\mu$ is the location parameter and $\sigma$ is decisive for the shape of the probability density function. Figure A.1 plots the probability density function for a fixed values of $\mu = 0$ and a selection of different values of $\sigma$. When comparing the shape of the log-normal distribution against the normal-distribution we notice their obviouse difference. We can see that the log-normal distribution is nonsymetrically with a skew to the left.

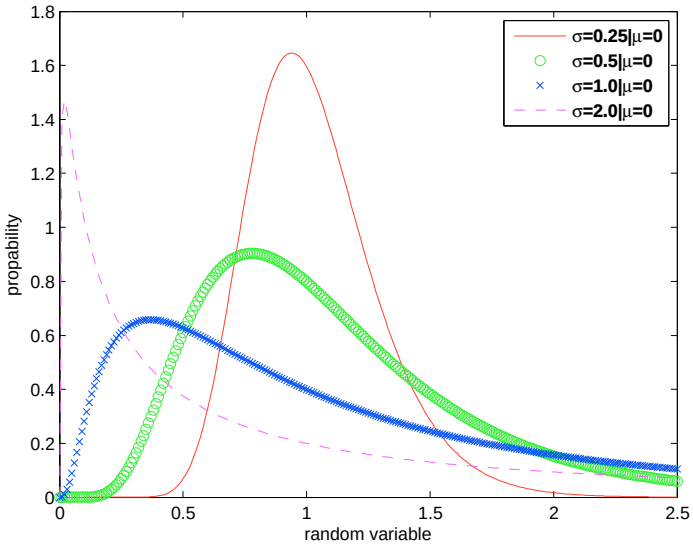


Figure A.1: Probability density function of the log-normal distribution (variable $\sigma$)

To complete the picture the figure A.2 plots the probability density function for a selection of different values of $\mu$ while keeping $\sigma$ constant.

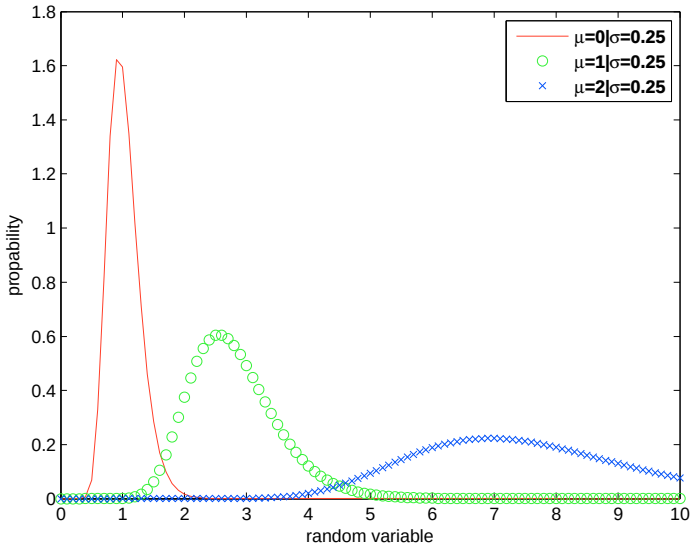


Figure A.2: Probability density function of the log-normal distribution (variable $\mu$)

## A.2 dB vs. dBm

dBm is a measure of power ratio in decibels which is referenced to 1 milliwatt. Some areas of application require the representation of a large range of values. With the use of the power ratio measure in dBm we can represent the dynamic range of values in a compact form. Equation A.2 formally describes the conversion to dBm. Solving the equation for power in dB we end up with equation A.3.

$$P_{dBm} = 10 \cdot log10(1000 \cdot P) = 10 \cdot log10(P) + 30 = P_{dB} + 30 \tag{A.2}$$

$$P_{dB} = \frac{1}{1000} \cdot 10^{\frac{P_{dBm}}{10}} = 10^{\frac{1}{10} \cdot (P_{dBm} - 30)} \tag{A.3}$$

## A.3 Shunt-Series transformation

This section is focused the conversion of simple two port networks. We assume that the impedance can be decomposed into a ohmic part that is in series with a purely imaginary load. This topology is transformed into a parallel topology. In this case the ohmic load is parallel to a imaginary impedance. The process of this transform is visualized with the help of figure A.3.
As the next step we have to write down the complex impedance for both circuits that are depicted in figure A.3. This yields the equation that is found in A.4.

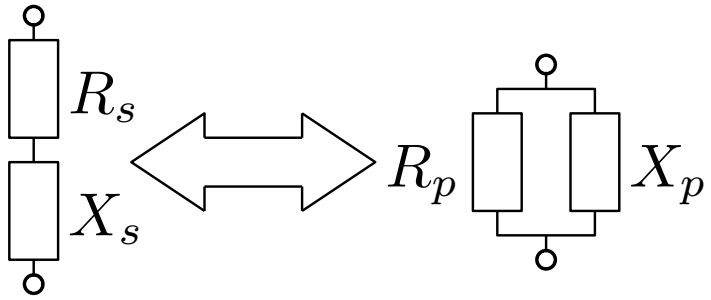


Figure A.3: Received power as a function of the distance (logarithmic scale)

$$\begin{aligned} R_s + jX_s &= \frac{R_p \cdot jX_p}{R_p + jX_p} = \frac{R_p \cdot jX_p}{R_p + jX_p} \cdot \frac{R_p - jX_p}{R_p - jX_p} \\ &= \frac{R_p \cdot X_p^2 + jX_p \cdot R_p^2}{R_p^2 + X_p^2} = \frac{R_p \cdot X_p^2}{R_p^2 + X_p^2} + j\frac{X_p \cdot R_p^2}{R_p^2 + X_p^2} \end{aligned} \tag{A.4}$$

As for now our system of equations is underdetermined. We need an additional information in the form of an additional equation that lets as convert the circuit topology. By introducing the quality factor $Q_s$ we get:

$$Q_s = \frac{X_s}{R_s} = \frac{R_p^2 \cdot X_p}{R_p \cdot X_p^2} = \frac{R_p}{X_p} = Q_p = Q \tag{A.5}$$

Making use of equation A.5 we can calculate the missing values of the new topology. Based on the objective that we want to achieve the identical impedance for a given frequency we can expect the same impedance on both sides of equation A.4. This implies that the real and the imaginary parts are identical. Hence we can use this fact to deduce an equation that allows us the calculate the values of the new topology. In our case we initally started with the series topology (left side of figure A.3) and derived the values for the parallel circuit (right side of figure A.3).
Comparing the real part of the left and the right hand side we get:

$$\begin{aligned} R_s &= R_p \cdot \frac{X_p^2}{R_p^2 + X_p^2} \\ &\rightarrow R_p \cdot X_p^2 = R_s \cdot (R_p^2 + X_p^2) \\ &\rightarrow R_p = \frac{R_s \cdot R_p^2}{X_p^2} + \frac{R_s \cdot X_p^2}{X_p^2} \\ &\overset{\frac{R_p}{X_p}=Q}{=} R_p \cdot (Q^2 + 1) \end{aligned}$$

The same holds to for the comparison of the imaginary parts of the equation in A.4:

$$
\begin{aligned}
X_s &= X_p \cdot \frac{R_p^2}{R_p^2 + X_p^2} \\
&\rightarrow X_p \cdot R_p^2 = X_s \cdot (R_p^2 + X_p^2) \\
&\rightarrow X_p = \frac{X_s \cdot R_p^2}{R_p^2} + \frac{X_s \cdot X_p^2}{R_p^2} \\
&\overset{\frac{X_p}{R_p}=Q^{-1}}{=} X_p \cdot (1 + Q^{-2}) \overset{Q\gg}{\approx} X_p
\end{aligned}
$$